2013

A Mathematical System for Human Implantable Wound Model Studies

Salomonsky Paul-Michael
Virginia Commonwealth University

.

College of Humanities and Sciences
Virginia Commonwealth University

This is to certify that the thesis prepared by Paul-Michael Salomonsky titled "A Mathematical System for Human Implantable Wound Model Studies" has been approved by his or her committee as satisfactory completion of the thesis requirement for the degree of Master of Science.

Rebecca Segal, Ph.D., College of Humanities and Sciences

Angela Reynolds, Ph.D., College of Humanities and Sciences

Robert F. Diegelmann, Ph.D., School of Medicine

Norma Ortiz-Robinson, Ph.D., Interim Graduate Chair, Mathematics and Applied Mathematics

---

Jim Coleman, Ph.D., Dean, College of Humanities and Sciences

F. Douglas Boudinot, Ph.D., Graduate Dean

Date

A Mathematical System for Human Implantable Wound Model Studies

A thesis submitted in partial fulfillment of the requirements for the degree of Master of Science at Virginia Commonwealth University.

by

Paul-Michael Salomonsky
Master of Science

Director: Rebecca Segal, Ph.D., Associate Professor
Department of Mathematics and Applied Mathematics

Virginia Commonwealth University
Richmond, Virginia
August 2013

Contents

List of Tables

List of Figures

Abstract

A MATHEMATICAL SYSTEM FOR HUMAN IMPLANTABLE WOUND MODEL STUDIES

By Paul-Michael Salomonsky, Master of Science.

A thesis submitted in partial fulfillment of the requirements for the degree of Master of Science at Virginia Commonwealth University.

Virginia Commonwealth University, 2013.

Director: Rebecca Segal, Ph.D., Associate Professor, Department of Mathematics and Applied Mathematics.

Dermal wound healing involves a myriad of highly regulated and sophisticated mechanisms, which are coordinated and carried out via several specialized cell types. The dominant players involved in this process include platelets, neutrophils, macrophages and fibroblasts. These cells play a vital role in the repair of the wound by orchestrating tasks such as forming a fibrin clot to stanch blood flow, removing foreign organisms and cellular debris, depositing new collagen matrix and establishing the contractile forces which eventually bridge the void caused by the initial infraction.

Our current understanding of these mechanisms has been primarily based upon animal models. Unfortunately, these models lack insight into pathologic conditions, which plague human beings, such as keloid scar or chronic ulcer formation. Consequently, investigators have proposed a number of *in vivo* techniques to study wound repair in humans in order to overcome this barrier. One approach, which has been devised to increase our level of

understanding of these chronic conditions, involves the cutaneous placement of a small cylindrical structure within the appendage of a human test subject.

Researches have designed a variety of these implantable structures to examine different aspects of wound healing in both healthy subjects and individuals that experience some trauma related condition. In each case, several implants are surgically positioned at multiple locations under sterile conditions. These structures are later removed at distinct time intervals at which point they are histologically analyzed and biochemically assayed to deduce the presence of biological markers involved in the repair process. Implantable structures used in this way are often referred to as Human Implantable Models or Systems.

Clinical studies with implantable models open up tremendous opportunities in fields such as biomathematics because they provide an experimentally controlled setting that aids in the development and validation of mathematical models. Furthermore, experiments carried out with implants greatly simplify the mathematics required to describe the repair process because they minimize the modeling of complex features associated with healing such as wound geometry and the evolution of contractile forces.

In this work, we present a notional mathematical model, which accounts for two fundamental processes involved in the repair of an acute dermal wound. These processes include the inflammatory response and fibroplasia. Our system describes each of these events through the time evolution of four primary species or variables. These include the density of initial damage, inflammatory cells, fibroblasts and deposition of new collagen matrix. Since it is difficult to populate the equations of our model with coefficients that have been empirically derived, we fit these constants by carrying out a large number of simulations until there is reasonable agreement between the time response of the variables of our system and those reported by the literature for normal healing. Once a suitable choice of parameters has been made, we then compare simulation results with data obtained from

clinical investigations. While more data is desired, we have a promising first step toward describing the primary events of wound repair within the confines of an implantable system.

Background

1.1 Wound Repair Biology

All dermal wounds primarily heal via three fundamental mechanisms. These include the deposition of new connective tissue, epithielization and contraction [1]. Although these actions constitute a majority of the healing process, they are by no means the only factors involved in the repair. In order for the body to effectively mitigate the damage caused by an injury, it must also mount an immune response, and it must replenish the supply of blood to the wound through a process know as angiogenesis [2]. Together these mechanisms are critical for removing debris and invasive organisms from the wound as well as providing basic nutrients which support the various aspects of wound repair. Each of these fundamental processes takes place during four highly regulated yet overlapping phases. These phases are referred to as hemostasis, inflammation, proliferation and remodeling [2], [3]. We discuss each of these phases in further detail in the following sections.

1.1.1 Hemostasis

Before the healing cascade can take place, blood flow, which occurs as a result of damage to blood vessels, must be stopped and a protective barrier must be put in place to shield the wound from potentially harmful agents. These events take place during the initial phase of wound healing known as hemostasis. During this period, platelets and other cell types flow out of damaged capillaries or blood vessels. As these cells are swept into the wound site, they come into direct contact with damaged components of the extracellular matrix. Here,

circulating platelets bind directly to exposed regions of the damaged matrix and to each other via collagen specific glycoproteins [4]. This interaction causes platelets to release a wide variety of compounds that not only initiate coagulation, but act as chemoattractants for cells that are involved in the inflammatory and proliferation phases.

Platelets initiate the clotting of blood through the release of clotting factors. These elements are stored in granules located within these cells, and they are dispensed near the site of damaged endothelium [4]. Clotting factors first trigger a coagulation cascade by the formation of cross-links between glycoproteins located on adjacent platelets. This facilitates the aggregation of platelets about the region of damaged endothelium. In turn, clotting factors along with a plethora of other agents contained in the serum component of blood trigger a complex sequence of biochemical pathways that eventually lead to the formation of an insoluble fibrin clot [1]. Once formed, the clot serves as a provisional barrier, which stanches blood flow and protects the site of injury until a new collagen matrix can be synthesized.

In addition to clotting agents, platelets, once activated, also serve as the initial source of a number of growth factors or cytokines. These peptides promote various aspects of the healing response such as inflammation, angiogenesis and fibroblast recruitment. During hemostasis, these cells produce a wide variety of cytokines which include platelet-derived growth factor (PDGF), basic fibroblast growth factor (FGF), transforming growth factor beta (TGF-β), and vascular endothelial growth factor (VEGF) [1], [2], [3]. Among these agents, PDGF and TGF-β probably serve as the most powerful chemical cues by establishing gradients which are fundamental for the chemotaxis of cells involved in the inflammatory response as well as those which carry out the repair of the damage extracellular matrix. In this regard, PDGF initiates the chemotaxis of neutrophils, macrophages and fibroblasts. It also promotes the cellular division of fibroblasts and smooth muscle cells thereby increasing their numbers. TGF-β, in turn, provides a secondary mechanism for the recruitment of

macrophages. This growth factor also causes immune cells, which are resident within in the surrounding tissue of the wound, to release several proinflammatory cytokines. The combined affect of these signals setups a vigorous immune response which marks the onset of the inflammation phase.

1.1.2 Inflammation Phase

The inflammation phase begins with the active recruitment of polymorphonuclear leukocytes or neutrophils. This is a complex process and takes place within the first 24 hours post-injury [1],[5], [6]. During hemostasis, the release of proinflammatory cytokines such as interleukin 1 (IL-1) and tumor necrosis factor alpha (TNF-α) lead to the formation of receptor molecules which are expressed on the outer surfaces of endothelial and neutrophil cell walls [7]. These receptors are referred to as adhesion molecules. They can be placed into two categories. These include adhesins, which endothelial cells express, and integrins, which reside on the surfaces of neutrophils. The interaction between these two molecules leads to the aggregation of neutrophils along the endothelium in the vicinity of wound [8]. Once neutrophils adhere to these active sites, they migrate across the endothelial barrier and follow cytokine gradients into the wound site. Neutrophils attain their maximal numbers within 24-48 hours after injury [5], [9]. In the absence of appropriate stimuli, neutrophils stop migrating. This occurs approximately 72 hours after injury [5], [9].

Another important cell type which emerges during the inflammatory phase is the mast cell. Mast cells are widely distributed throughout the connective tissue of the body. When surfaces of these regions are exposed during injury, mast cells degranulate thereby releasing their contents[10]. Consequently, mast cell numbers fall sharply immediately following an injury. Mast cell levels return to normal levels after approximately 48 hours after the onset of injury. During this process, mast cells release a number of proinflammatory mediators which promote vascular changes in the vicinity of the wound. The mediators released by mast cells

are responsible for the characteristic signs of inflammation. These include Rubor (Redness), Calor (Heat), Tumor (Swelling) and thus Dolor (Pain). Mast cells have been reported to release TNF-α, macrophage inflammatory protein-2 (MIP-2) and IL-8, as well as histamine, and other amines [1]. The net affect of these actions causes blood vessels and surrounding tissue to become porous. This phenomena supports the infiltration of neutrophils into the wound and produces the characteristic signs of inflammation that accompany most injuries.

Macrophages are the last cell type to arrive in the wound during the inflammatory phase. These cells represent another very important class of immune cells that are involved in the healing cascade. Macrophages act to reinforce the actions of neutrophils. Macrophages also serve to remove expended neutrophils from the wound. These cells appear approximately 48 hours after injury [1], [5]. Macrophages initially exist in the form of fixed tissue monocytes, which reside in regions of contiguous healthy tissue. These cells become activated via exposure to the cytokines that are released during hemostasis. Like neutrophils, they migrate along cytokine gradients via chemotaxis until they arrive at the wound site.

Once neutrophils and macrophages arrive at the site of injury, these inflammatory cells perform the crucial task of cleaning the wound. As part of this assignment, these cells remove foreign material, dead host cells and components of the damaged extracellular matrix. If pathogens are present within the wound, inflammatory cells also act by eliminating these invasive organisms. Inflammatory cells are attracted to these microorganisms through the release of a specific peptide marker, f-Met-Leu-Phe, which is a byproduct of bacteria protein synthesis [1].

Inflammatory cells clean the wound through a process known as phagocytosis. During this process, immune cells ingest large quantities of their prey by engulfing them into structures referred to as lysosomes. These structures contain harmful proteolytic agents which digest material by breaking down its protein structure. Eventually, inflammatory cells succumb to the powerful effects of these proteolytic enzymes after removing debris and

other matter from the wound. The end product of this process can often be visualized in the form of "pus" which emanates from most dermal wounds [1].

In addition to cleaning the wound, inflammatory cells also reinforce the cytokine gradients initiated during hemostasis. Macrophages are primarily responsible for this action through the release of PDGF and TGF-β. These signals not only stimulate migration of immune cells but they eventually draw fibroblasts and smooth muscle cells to the wound. The appearance of macrophages signifies that the inflammatory phase is drawing to a close [1]. For acute dermal wounds, the inflammatory response typically last for approximately one week following an injury [2], [3], [5].

1.1.3 Proliferation Phase

Chemical gradients, which are first established by platelets during hemostasis and later reinforced by immune cells during inflammation, eventually lead to fibroblast recruitment to the wound. These cells initially appear in the wound 2-3 days after injury [11], [12], and their arrival signifies onset of the proliferation phase.

Proliferation is the most involved of all phases in wound healing because there are number of complex processes which take place during this period. Each of these subprocesses functions to support a specific aspect of repair. These processes include angiogenesis, epithielization, fibroplasia, and contraction [1], [2], [3]. In the context of this work, we primarily focus on the events associated with fibroplasia; however, we briefly touch on each of these areas to provide a comprehensive picture of the mechanisms involved in proliferation.

Angiogenesis

Blood supply to the wound is critical for repair. This precludes the emergence of environmental factors that can negatively impact the repair process. For instance, the function of

fibroblasts and epithelial cells can not proceed in an hypoxic environment. Furthermore, the lack of nutrients and the presence of lactic acid both of which accompany most wound environments also inhibit the ability of these cells to perform vital tasks associated with the healing cascade [1]. Neovascularization or angiogenesis is the process that replenishes blood flow to the wound by eliminating oxygen deprivation, replenishing nutrients and mitigating acidic conditions. During angiogenesis, intact capillaries generate buds which stem off into the wound. This process works in conjunction with fibroplasia because fibroblasts and epithelial cells require a rich oxygen environment with nutrients to preform their tasks.

Several cells play a role in the modulation of neovascularization. When macrophages, endothelial cells and fibroblasts experience a low oxygen, lactic acid dominated environment, they release vascular endothelial cell growth factor (VEGF), basic fibroblast growth factor (bFGF) and TGF-β [1]. These cytokines promote angiogenesis. As antagonistic conditions subside, these same cells stop their production of these important angiogenic factors.

Epithielization

Epithielization involves the replenishment of the outer layer of the skin or epidermis. This process is similar to epidermal wound healing. In epidermal wounds, keratinocytes or epidermal cells spread across the surface of the damaged epidermal layer of the skin [13]. At first, there is no immediate increase in the rate of cell generation above normal mitotic levels. The migration of keratinocytes simply involves the spreading out of these cells; however, shortly after the migration begins, keratinocytes near the wound edge experience an increase in their mitotic activity due to the loss of contact inhibition. This mechanism provides a new supply of keratinocytes [15] to the damaged epidermal region. In the case of an acute dermal wound, these cells travel from the periphery of the wound underneath the fibrin structure using granulation tissue for support. Wound edges are not the only source of epithelial cells. Sebaceous glands, sweat glands, and hair follicles, which remain intact after

injury, also serve as sources of keratinocytes. The onset of epithielization depends upon the extent of the wound. In larger wounds, this process can take longer periods to manifest itself because epithelial cells require granulation tissue to support their migration; however, epithielization may occur as soon as one day following injury.

As with neovasularization, macrophages and platelets play a key role in the regulation of epithielization. Keratinocytes also assist in the modulation of this process. Each of these cell types release two essential cytokines that stimulate cell division. These factors are epidermal growth factor (EGF) and transforming growth factor alpha (TGF-α) [1]. The spreading of keratinocytes commences immediately following an injury; however, the division of peripheral cells occurs after sufficient levels of EFG and TGF-α have been established. Once a layer of epithelial cells has formed beneath the provisional matrix, these cells release several enzymes which breakdown this structure eventually leading to its removal.

Fibroplasia

During the proliferation phase, fibroblasts become the main focal point in the repair process, and fibroplasia signifies the process where these cells provide their main function with respect to wound healing.

As the inflammatory phase begins to wane, fibroblasts primarily undergo mitotic generation and migrate from nearby connective tissue. In this regard, PDGF and TGF-β serve as essential control mechanisms by promoting cell division and chemotaxis [1]. After 1-2 weeks, fibroblast levels resulting from these two activities begin to peak [5], [12], and these cells become the dominant players within the wound. TGF-β also provides an additional role with respect to fibroblast. During fibroplasia, this growth factor becomes a very important signal which promotes a slew of fibroblast gene transcription products. Here, TGF-β stimulates the expression of glycosaminoglycans, proteoglycans, glycoproteins and most notably collagen [1].

Fibroblast transcription products serve as components for the new extracellular matrix. Glycosaminoglycans, proteoglycans, glycoproteins are often referred to as ground substance. Ground substance constitutes the non-collagen part of the extra-cellular matrix which promotes the growth of granulation tissue. Granulation tissue consists of a host of new cells such as fibroblasts, myofibroblasts, endotheliel cells and macrophages. Alternatively, collagen provides structure and serves as the primary source of tensile strength in newly deposited connective tissue. In contrast, the provisional fibrin clot is quite week and is highly susceptible to trauma. The deposition of new collagen typically levels off approximately 2-3 weeks after injury [5] depending on the nature of the wound. During this period, collagen production eventually reaches an equilibrium where its degradation and production become balanced. When this occurs, fibroblasts undergo apoptosis [11], returning to their normal levels in healthy tissue. At this point, fibroplasia draws to a close.

Wound Contraction

If a wound can be closed by some surgical technique, then the wound primarily heals through the deposition of new connective tissue. However, if a wound remains open, then it requires contractile forces to close. This is often referred to as wound contraction. In clinical terms, the former process is known as healing through primary intention where as the later case is called healing by secondary intention. The mechanisms involved in wounds that heal through secondary intention are not well understood; however, it has been established that contraction involves the interaction between specialized cells called myofibroblasts and components of the extracellular matrix [1]. During the later stages of proliferation, fibroblasts differentiate into myofibroblasts. The mechanisms associated with this transition are unclear; however, growth factors are thought to play a vital role. The differentiation of fibroblasts leads to the expression of actin and myosin, which are two important contractile proteins. It has long been know that the actin-myosin complex facilitates contraction in

smooth muscle cells, and this association provides the same contractile mechanism within myofibroblasts.

As myofibroblasts appear in the wound, they begin to form linkages with each other and components of the extra-cellular matrix. These interconnections lead to a network which extends throughout the wound to its perimeter. As these cells contract the wound is pulled shut. The contractile forces associated with the actin-myosin complex begin during the first week of the healing; however wound contraction is a slow process which can last up to several weeks well after the onset of injury extending this process into the remodeling phase.

1.1.4 Remodeling Phase

When the decay and production rates of collagen reach a steady state, the process of collagen remodeling begins. This period is often referred to as maturation or remodeling. It is the last phase that occurs during wound repair.

After approximately three weeks, collagen deposited during the proliferation phase begins to undergo further processing. Specialized enzymes, which are produced by fibroblasts, start to breakdown type III collagen and replace it with type I collagen [2]. This replacement continues until there is respectively a 4:1 ratio of type I to type III collagen. These new structures are cross-linked and then aligned with existing components of the extracellular matrix. Enzymes, such as lysyl oxidase, act on the new collagen to form these stable cross-links [1].

Collagen remodeling can last for years after the injury [9]. Over this period, more intramolecular and intermolecular cross-links are created. This gives the new collagen matrix strength and stability; however, the wound never fully regains its total functionality. The maximum strength provided by new collagen plateaus at approximately 80% of normal tissue [1].

1.2 Mathematical Models of Wound Repair

There are a wide variety of mathematical systems that have been proposed to describe the fundamental processes associated with the repair of a cutaneous wound. These models range in their level of complexity based upon the degree to which they incorporate key mechanisms associated with a given aspect of repair. For example, many models only account for a subset of the mechanisms involved with a particular wound healing process such as fibroplasia or epithielization. Often these models require mathematical apparatus to account for the underlying mechanisms such as cell mitosis and death, capillary tip formation, oxygenation, growth factor induced chemotaxis and mitogenesis, collagen matrix deposition and/or wound contraction. In this section, we provide a brief account of mathematical systems that have been proposed to account for the various aspects of wound repair. This is by no means an comprehensive list, but it provides a context of the important work that has already been establish toward mathematically modeling cutaneous wounds.

Thackham et al. [17] investigated several in silico approaches for solving different types of advection-dominated models. These models attempt to described a subset of the events involved in angiogenesis. Although their work primarily focuses on the suitability of numerical techniques for solving the equations that arise from wound healing, they present several systems of partial differential equations (PDEs) which account for angiogenesis. These PDE systems model neovasularization by accounting for the development of either endothelial cell or capillary tip density in response to chemotactic mediators such as VEGF. In their investigation, they analyze several wound healing scenarios in both one and two dimensions; however, they do not attempt to describe the repair process beyond the confines of neovascularization.

Menke et al. [18] have focused on a more complete repair model by using an integrated systems approach to describe the repair process in hypoxic environments. Their work

focuses on the extension of a system of ordinary differential equations (ODEs) originally proposed by Reynolds et al. [19]. Reynolds et al. originally created their system to describe the acute inflammatory response at a systemic level. This system was modified by Menke et al. to include fibroblast activity and incorporate tissue oxygenation producing a wound repair system. The result consists of a set of ODEs which account for tissue damage, inflammation, fibroblasts and pathogen level. Although the model is able to account for the effects of low tissue oxygenation in the presence of varying degrees of contamination, it lacks a spatial component which describes the evolution of each species within the wound geometry during the repair process.

Sherratt and Murray [20], [21] created a wound healing model consistent with the repair of the epidermis. They implement a Fickian diffusion model which incorporates stimulus for increase in epidermal mitosis through an activator/inhibitor mechanism. Their work illustrates that the biochemical regulation of mitosis through chemical activation or inhibition plays a key role in the repair process. Although simulations with their model compare well with empirical results, the model does not account for events which occur in full depth wounds.

Vermolen et al. [22] model a particularly problematic aspect of wound repair, namely wound contraction. Their work focuses on closure of the wound mediated through growth factor controlled tissue regeneration. In their work, a wound healing rate equation is combined with a reaction transport equation within an active layer adjacent to the wound where growth factor is produced. Tissue regeneration and expansion of the active layer proceeds if the concentration of growth factor exceeds a certain threshold value. Their work builds upon a set of mathematical models for wound healing first presented by Adam [23]. These models [23]-[25] primarily focus on the Critical Size Defect (CSD) associated with a wound. CSD is defined as the smallest wound that does not heal within the lifetime of a test subject. Although their model accounts for this difficult aspect of repair, they do not

account for other fundamental repair processes such as inflammation or tissue oxygenation which directly affect the rate of healing.

Xue et. al. [26], [27] present an extensive model of the repair of ischemic cutaneous wounds. Their system accounts for several aspects of wound repair including wound contraction. Their system of equations consists of a set of coupled of PDEs in the partially healed region modeling the wound edge as a free boundary. The free boundary moves with the velocity of the the extracellular matrix (ECM) at the wound edge. The system of equations model the concentration oxygen and cytokines such as PDGF and VEFG. The model also contains terms for macrophage, fibroblasts, capillary tip density as well as ECM velocity. Simulations of their model demonstrate that ischemic conditions limit macrophage recruitment to the wound-site and impair wound closure.

1.3 Implantable Systems

Although a wide variety of wound repair models currently exist, researchers have not proposed a wound healing model that describes the various aspects of repair within the context of a human implantable model. Clinical investigators have devised these systems in order to gain insight into mechanisms associated with abnormal repair in human beings. This is because animal models, which are currently used in clinical investigations, lack insight into abnormal healing states, which plague humans. For example, Seok et. al. have shown that acute inflammatory stresses in hummans produced from different causes correlate poorly with mouse models [16]. Humans have a tendency to exhibit either excessive or deficient healing [28]. These extremes pronounce themselves in the form of keloids and hypertrophic scar formations or chronic ulcers, respectively.

Implantable systems are porous cylindrical structures that are surgically placed within the cutaneous layer of the skin. In clinical investigations, multiple implantable structures

are positioned at distinct locations through out a test subject's appendage [29]. The surgical procedures used to position an implant are carried out under aseptic conditions in order to prevent infection. Hence, the immune response associated with these injuries is geared entirely toward the removal of cellular debris and damaged matrix components produced during implantation.

Once surgically positioned, implants are removed at distinct times points, at which time they are assayed for biological markers that characterize the phase of repair as well as the processes involved in the healing response [28]. Examinations often include differential cell counts, which determine the presence and quantity of neutrophils, macrophages and fibroblasts, as well as biochemical assays, which determine the amount of collagen deposited in the wound.

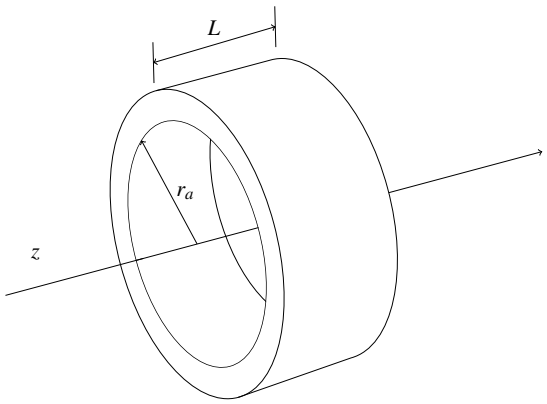

Figure 1.1: Conceptual diagram of a synthetic implant

Researchers have developed a variety of these *in vivo* models. The design of each of these systems has evolved over time. Although these implantable systems can be employed to examine different aspects of the healing process, they all conform to an overall cylindrical design as illustrated by Figure 1.1. Here, the inner region indicated by r_a may be empty as in the case of the Schilling-Hunt steel mesh chamber, or it may be filled with viscose cellulose sponge (Cellstick model) [28]. In other synthetic implantable wound healing systems, the

inner region may represent a contiguously integrated matrix composed entirely of polyvinyl alcohol (PVA) or polytetrafluoroethylene (ePTFE) sponge [28], [29].

The Implantable PDE Model

An acute dermal wound generally proceeds through a well orchestrated sequence of events all of which lead to the restoration of normal anatomic structure and function. In this work, we seek to account only for a subset of these events. We primarily focus on the inflammatory response and events that occur during fibroplasia. In order to describe these events, our model consists of a set of four conservation equations, which describe the time rate of change of the density of damaged tissue, inflammatory cells, fibroblasts and newly deposited collagen matrix.

We use a number of well-established mathematical techniques to describe both the physical and biological processes involved in the repair process. The underlying mathematical building blocks we use include

1. the Logistic Equation - models population growth,
2. first order kinetic models - account for population death or decay rates,
3. the Mass Action Law - models interactions between reactive species,
4. the Keller-Segel model - accounts for cell chemotaxis.

Using these well established modeling techniques, our wound repair system is as follows

$$\frac{\partial m}{\partial t} = -\mu_{mn} mn, \tag{2.1}$$

$$\frac{\partial n}{\partial t} = \nabla \cdot [D_n \nabla n - n\chi_n \nabla m] - \mu_{nm} mn, \tag{2.2}$$

$$\frac{\partial f}{\partial t} = \nabla \cdot \left[D_f \nabla f - f\chi_f \nabla n\right] + s_f(n) f \left(2 - \frac{f}{F_0}\right) - \mu_f f \tag{2.3}$$

$$\frac{\partial c}{\partial t} = k_c f (C_0 - c) - \mu_{cn} cn \tag{2.4}$$

Here, $m(\vec{x},t)$, $n(\vec{x},t)$, $f(\vec{x},t)$ and $c(\vec{x},t)$ represent the density of damaged tissue, activated inflammatory cells, fibroblasts and new collagen deposition respectively where $\vec{x} \in \mathbb{R}^3$. In the following sections, we discuss the rationale behind each of these equations.

2.1 Origins of Keller-Segel System

Many of the mathematical models that we use in our wound repair system are standard techniques. For example, first order kinetics have long been used to describe decay processes at the molecular level. They have also been introduced to describe the production of biological agents. Furthermore, chemists have used the Law of Mass Action to describe chemical reactions between two species which interact to form products of the reaction. These techniques are often used to describe the rates of production or degradation (sources and sinks, respectively) in mathematical models.

The Keller-Segel model provides a kinematic term. This system has been used to describe the reaction-diffusion of species that undergo chemotactic motion in response to a stimuli [17], [30], [31]. For this reason, we have implemented this system to account for the chemotaxis of fibroblast and inflammatory cell populations. From a mathematical perspective, it is difficult to ascertain the mechanisms behind this model when implemented

in a system of equations. In order to add context to this mathematical form, we present a concise derivation of this important system.

It is important to note that although this system was first developed by Evelyn Keller and Lee Segel in 1970 [32]-[34], it has generated a great deal of interest since its inception. Consequently, researches have made modifications to it in pursuit of their specific interests. We implemented this system based upon the research provided by Hillen and Painter [35]. Although Hillen et al. derive this system using a semi-discrete probability approach, we arrive at the system using a more classical analysis.

Consider the cell density u, normal diffusive processes consider the flux as

$$\vec{J}_d = -D_u \nabla u.$$

However, for a chemotactic system, we have

$$\vec{J} = \vec{J}_d + \vec{J}_c = -D_u \nabla u + u\chi_u \nabla v,$$

where v is a chemical. The first term is due to random motion of u, where as the second term, $\vec{J}_c$, is due to chemotaxis. The later term just states that the chemotactic flux, $\vec{J}_c$, is proportional to the concentration of u and the vector field ∇v, or the gradient of v. Now, the mass balance of u through an arbitrary control volume is given by

$$\frac{d}{dt}\iiint_V u dV = -\oiint \vec{J}\cdot\hat{n} dS + \iiint_V f_u(u,v) dV,$$

here $f_u(u,v)$ represents sources and sinks (i.e. cell mitosis and cell death terms of u), which we drop for convenience. Therefore this becomes

$$\frac{d}{dt}\iiint_V u dV = -\oiint \vec{J}\cdot\hat{n} dS,$$

Applying the Divergence Theorem, we have

$$\frac{\partial u}{\partial t} = -\nabla \cdot \vec{J} = \nabla \cdot (D_u \nabla u - u\chi_u \nabla v)$$

Since v obeys purely random motion, by similar logic we have

$$\frac{\partial v}{\partial t} = -\nabla \cdot \vec{J}_d + f_v(u,v) = D_v \nabla^2 v + f_v(u,v),$$

where f_v is often taken as $ku - \mu v$ [35]. This analysis gives the Keller-Segel model, which we restate below for convenience

$$\begin{aligned} \frac{\partial v}{\partial t} &= D_v \nabla^2 v + f_v(u,v), \\ \frac{\partial u}{\partial t} &= \nabla \cdot (D_u \nabla u - u\chi_u \nabla v) \end{aligned}$$

2.2 Damage Marker Equation

Damage may be interpreted as the adulteration of the wound by foreign material and the destruction of functional tissue such as collagen matrix. We view tissue damage as fixed in space or having a time scale that is relatively slower than the chemotaxis of inflammatory cells and fibroblasts. Hence, we do not account for the diffusion of damaged tissue or foreign debris in the wound. In addition, we make the assumption that the injury is a result of a surgical incision which occurs under sterile conditions. Therefore, we do not account for the presence of pathogen in this model.

It is the immune systems responsibility to remove debris from the wound during the healing process. Inflammatory cells, such as neutrophils and macrophages, carry out this function by engulfing debris and digesting it in lysosomes through a process known as

phagocytosis. Inflammation also leads to harmful side effects. As inflammatory cells enter the wound to remove damaged tissue, they also damage healthy functional tissue. This side effect can become pronounced during abnormal repair where inflammation lasts longer. In our work, we do not model this side effect.

The damage equation consists of a conservation equation for initial tissue damage, $m(\vec{x},t)$, stemming from the initial injury. From a conservation of mass perspective, the damage equation in our wound healing model may be expressed as follows

$$\begin{pmatrix} \text{Rate of removal} \\ \text{of initial tissue damage} \end{pmatrix} = \begin{pmatrix} \text{Rate of removal} \\ \text{by phagocytosis} \end{pmatrix}.$$

We account for phagocytosis through a reaction based mechanism. This process may be described by the following reaction

$$m + n \rightarrow n^*,$$

where m, n and n^* represent the density of initial damaged tissue, inflammatory cells and inactive inflammatory cells. Essentially, this equations depicts the process where by an activated inflammatory cell removes damaged tissue from the wound. The result is an inactive inflammatory cell. When we refer to the term n^*, we mean a inflammatory cell that has succumbed to proteolytic processes that were vital in removing non functional tissue. The Law of Mass Action states that the rate of removal of debris is proportional to the density of damaged tissue and inflammatory cells within the wound. This is represented in mathematical terms using the following differential equation:

$$\frac{dm}{dt} = -\mu_{mn} mn. \tag{2.5}$$

Here, μ_{mn} is the consumption rate of damaged tissue by inflammatory cells. This quantity is

expressed in units of volume $\cdot$ time^{-1}, where we express time in days. Note that Equation (2.5) is equivalent to (2.1). That is the rate of removal of $m(\vec{x},t)$ has no spatial dependence with respect to the wound healing process. Therefore, we can express this as

$$\frac{\partial m}{\partial t} = -\mu_{mn} mn.$$

2.3 Inflammation Equation

Inflammatory cells, such as neutrophils and macrophages, typically respond to damage via autocrine and paracrine mechanisms. These mechanisms are mediated through the release of peptides referred to as cytokines. Two cytokines involved in wound repair at the onset of injury include PDGF and TGF-β. Inflammatory cells travel along gradients produced by these cytokines through a process known as chemotaxis. As these cells arrive in the wound, they begin consuming non-functional host tissue and foreign debris through phagocytosis. Eventually, inflammatory cells succumb to the same proteolytic processes that they employ to clean the wound. We view the overall rate of change of inflammatory cells in the wound as the sum of these two processes. In general terms, we have

$$\begin{pmatrix} \text{Rate of change of} \\ \text{inflammatory cell density} \end{pmatrix} = \begin{pmatrix} \text{Inflammatory cell} \\ \text{chemotaxis} \end{pmatrix} - \begin{pmatrix} \text{Inflammatory cell death} \\ \text{from phagocytosis} \end{pmatrix}.$$

In our model, we account for inflammatory cell chemotaxis; however, we do not account for chemotaxis by way of chemical cues such as PDGF and TGF-β. Instead, we assume these mediators, initially released by platelets at the onset of injury, form a gradient that is proportional to the initial tissue damage, $m(\vec{x},0)$. We assume this proportionality holds as the cytokine gradient changes with respect to time. In other words, if $\phi(\vec{x},t)$ represents the

density of cytokines, then $m = K\phi$ for all $t > 0$ where K is a positive constant. Hence, in our model, inflammatory cells respond to the evolution of the damage gradient, $m(\bar{x},t)$.

We draw inspiration from the Keller-Segel chemotaxis model [32] - [34] to account for inflammatory cell chemotaxis. As described above, this system consists of the following two partial differential equations:

$$\begin{aligned} \frac{\partial v}{\partial t} &= D_v \nabla^2 v + f_v(u,v), && (2.6) \\ \frac{\partial u}{\partial t} &= \nabla \cdot [D_u \nabla u - u\chi \nabla v] && (2.7) \end{aligned}$$

where $\nabla\cdot$ is the divergence of a vector field. Here, u denotes the cell density on a given domain $\Omega \subset \mathbb{R}^3$ and v describes the concentration of the chemical signal. D_v, k and μ represent the diffusion, rate of production and degradation of chemical, respectively. In Equation (2.7), χ is the chemotactic coefficient; D_u is sometimes referred to as the motility or diffusion constant. In our work, we couple the chemotaxis equation, Equation (2.7), to the damage equation, Equation (2.1), to model the immune response to tissue damage. The inflammatory chemotaxis system initially appears as

$$\begin{aligned} \frac{\partial m}{\partial t} &= -\mu_{mn} mn. \\ \frac{\partial n}{\partial t} &= \nabla \cdot [D_n \nabla n - n\chi_n \nabla m], && (2.8) \end{aligned}$$

where D_n and χ_n represent the diffusion and chemotaxis constants, respectively.

During phagocytosis, inflammatory cells eventually succumb to the same proteolytic processes that are responsible for the breakdown of foreign material and cellular debris within the wound. To account for their destruction, we implement the Law of Mass Action

once again. Consequently, the inflammatory cell death term due to phagocytosis resembles Equation (2.1) and is given as follows

$$\frac{\partial n}{\partial t} = -\mu_{nm} mn. \tag{2.9}$$

We should note that the death rate of inflammatory cells governed by the constant μ_{nm} is different than the rate constant μ_{mn} shown in Equation (2.1). Its units are the same; however, since a single inflammatory cell may engulf numerous quantities of cellular debris, we expect $\mu_{nm} < \mu_{mn}$. That is the rate of removal of inflammatory cells occurs at a slower rate than the removal of damaged tissue from the wound. The overall rate of change of inflammatory cells is the sum of Equations (2.8) and (2.9). Thus, we arrive at the overall time rate of change of inflammatory cells in the wound, which we restate below for convenience

$$\frac{\partial n}{\partial t} = \nabla \cdot [D_n \nabla n - n\chi_n \nabla m] - \mu_{mn} mn.$$

2.4 Fibroblast Equation

As inflammation subsides and inflammatory cells reduce in number, fibroblasts begin to enter the site of injury. This marks the beginning of the proliferation phase. During this period, fibroblasts respond to the same cytokine gradients as inflammatory cells, and they react to cytokines signals in two ways. First, cytokines provide chemical signals for fibroblast chemotaxis. Hence, these chemical cues influence fibroblast cell migration to the wound. Second, cytokines serve as important mitogenic agents causing fibroblasts to increase their rate of mitotic cell division. We account for both of these mechanisms in our wound repair model as well as the natural loss of fibroblast cells. Thus, the mass balance of fibroblast cell density is expressed as

$$\begin{pmatrix} \text{Rate of change of} \\ \text{fibroblast density} \end{pmatrix} = \begin{pmatrix} \text{Fibroblast} \\ \text{Chemotaxis} \end{pmatrix} + \begin{pmatrix} \text{Fibroblast mitotic} \\ \text{generation} \end{pmatrix} - \begin{pmatrix} \text{Fibroblast} \\ \text{cell death} \end{pmatrix}.$$

As with the inflammatory equation, we do not directly account for fibroblast chemotaxis via cytokine gradients. Rather, we assume that cytokines, which are produced by neutrophils and macrophages during inflammation, form gradients that are proportional to the density of these inflammatory cell populations. Therefore, fibroblasts respond to the evolution of the inflammatory cell gradient in our model. Once again, we use the Keller-Segel system to describe fibroblast chemotaxis. Here, the time rate of change of fibroblasts due to chemotaxis becomes

$$\frac{\partial f}{\partial t} = \nabla \cdot \left[D_f \nabla f - f \chi_f \nabla n \right],$$

where D_f is the diffusion or motility constant associated with fibroblasts, and χ_f is the chemotaxis constant. These constants have units of $space^2 \cdot time^{-1}$ and $space^5 \cdot time^{-1}$, respectively. In this equation, D_f and χ_f serve the analogous roles that D_n and χ_n provided in the inflammation equation.

To account for fibroblast cell growth, we use a logistic model. The Logistic equation has long been used to describe the growth rate of populations. It has the following general form

$$\frac{du}{dt} = ku\left(1 - \frac{u}{U_0}\right),$$

where k is a constant that depicts the growth rate and U_0 is the population's maximum sustainable value. All cell populations such as fibroblasts eventual experience apoptosis or cell death [11]. In order to account for the overall life cycle of fibroblasts within the wound,

we add the first order decay term, $-\mu_f f$, to account for cell death. Therefore, the time rate of change of fibroblasts associated with these two terms appears as

$$\frac{df}{dt} = s_f(n) f \left(2 - \frac{f}{F_0}\right) - \mu_f f. \tag{2.10}$$

Here, μ_f is a constant that describes the death rate of fibroblasts, and F_0 is the nominal density of fibroblasts in healthy tissue. These constants have units $time^{-1}$ and $volume^{-3}$, respectively. There is a subtle difference between the logistic equation and its implementation in Equation (2.10). In equation (2.10), we introduced the term $(2 - f/F_0)$ rather than $(1 - f/F_0)$. This factor was introduced to model the equilibrium condition of the fibroblast equation. That is we desire the mitotic generation rate and death rate of fibroblasts to balance as $t \to \infty$. We will discuss this subtlety in more detail in Section 2.6.

Since cytokines influence the mitogenic response rate of fibroblasts, the growth rate would normally be a function of cytokine concentration, or in our case, its proxy, inflammatory cell density. Hence, $s_f(n)$ serves as a variable mitogenic growth rate in Equation (2.10); however, for simplicity, we let $s_f(n) = k_f$. Combining both chemotaxis and cell life cycle terms produces the overall rate equation for fibroblasts during repair. This has the following form:

$$\frac{\partial f}{\partial t} = \nabla \cdot \left[D_f \nabla f - f \chi_f(f) \nabla n\right] + k_f f \left(2 - \frac{f}{F_0}\right) - \mu_f f$$

2.5 Repair Equation

The density of newly deposited collagen and granulation tissue is a direct indication of the progress of the repair. Any system that attempts to explain dermal wound repair must account for these variables. Thus, we monitor the status of these two species with a single unknown, $c(\vec{x}, t)$. Prolonged inflammation can damage newly deposited collagen and granulation tissue.

In our modeling approach, we account for damage to newly deposited tissue due to this mechanism. Consequently, our conservation equation results from the mass balance of these two terms. The overall time rate of change of the density of newly deposited tissue during wound healing is expressed as follows

$$\begin{pmatrix} \text{Overall rate of} \\ \text{new tissue deposition} \end{pmatrix} = \begin{pmatrix} \text{Fibroblast tissue} \\ \text{deposition rate} \end{pmatrix} - \begin{pmatrix} \text{Tissue damage rate} \\ \text{from phagocytosis} \end{pmatrix}.$$

First, we consider the rate of new collagen deposition to be proportional to the density of fibroblasts and collagen damage, $\widehat{c}$, in the wound. This gives

$$\frac{\partial c}{\partial t} = k_c f \widehat{c}, \tag{2.11}$$

where k_c is a positive constant which describes the rate of collagen deposition. This constant has units of $volume \cdot time^{-1}$. Collagen damage, $\widehat{c}$, can be expressed as the difference between the existing collagen density, C_0, in undamaged tissue and undamaged collagen, c, within the wound. In other words, we write

$$\widehat{c} = C_0 - c, \tag{2.12}$$

Substituting Equation (2.12) into (2.11) provides the rate of collagen deposition in the wound. This is given as

$$\frac{\partial c}{\partial t} = k_c f \left(C_0 - c\right). \tag{2.13}$$

Prolonged inflammation leads to tissue damage. Here, we account for damage to newly deposited collagen and granulation tissue by this mechanism using a mass action term. In

our repair equation, we view the rate of damage to new collagen matrix and granulation tissue as proportional to the product of the density of inflammatory cells and newly deposited tissue in the wound domain. This yields the following damage rate term:

$$\frac{\partial c}{\partial t} = -\mu_{cn} n c, \tag{2.14}$$

where μ_{cn} represents a positive rate constant for tissue damage due to inflammation. This rate constant has units $volume \cdot time^{-1}$. Combining Equations (2.13) and (2.14) yields the overall rate of repair or equation (2.15).

$$\frac{\partial c}{\partial t} = k_c f\,(C_0 - c) - \mu_{cn} n c, \tag{2.15}$$

2.6 The Repaired State

In humans, an acute dermal wound only regains approximately 80% of its original structural integrity with regards to tensile strength; however, in our model, we assume that the wound fully recovers. What does this state look like in terms of our model? If repair proceeds in a ideal manner, we expect all damaged tissue to be removed from the wound during the inflammatory phase. Inflammatory cells respond to specific biological markers or antigens which once removed, provide no stimuli for inflammatory cell functionality. Thus, activated inflammatory cell levels should drop as the density of damaged tissue disappears from the wound. Ideally, damaged matrix and inflammatory cell levels should both approach zero as the system approaches the final repaired state.

On the other hand, as repair proceeds, we expect the rate of newly deposited collagen matrix to slow as the newly deposited collagen and granulation tissue approaches their nominal values in healthy or undamaged tissue. In our wound repair system, we model this value as C_0, the density of healthy tissue. As collagen density recovers in the wound,

fibroblasts enter an equilibrium where their overall rate of production and death due to apoptosis balance around their nominal levels in normal tissue, F_0 [11]. Thus, in terms of all variables, we assume that the repaired state represents the point $(\bar{m},\bar{n},\bar{f},\bar{c}) = (0,0,F_0,C_0)$. With regard to our system of equations, this is a special point or solution to our model, if $k_f = \mu_f$.

Under these assumptions, if we let $(m,n,f,c) = (\bar{m},\bar{n},\bar{f},\bar{c})$, we have

$$\begin{aligned}
\frac{\partial \bar{m}}{\partial t} &= \mu_{mn} \cdot 0 \cdot 0 = 0, \\
\frac{\partial \bar{n}}{\partial t} &= 0 - \mu_{nm} \cdot 0 \cdot 0 = 0, \\
\frac{\partial \bar{f}}{\partial t} &= 0 + k_f \cdot F_0 \cdot (2 - \frac{F_0}{F_0}) - \mu_f \cdot F_0 = 0 \\
\frac{\partial \bar{c}}{\partial t} &= k_c \cdot f \cdot (C_0 - C_0) - \mu_{cn} \cdot 0 \cdot 0 = 0
\end{aligned}$$

In other words, the repaired state represents a homogeneous steady state solution in our system of equations.

Analysis of the Inflammation System

We model the acute inflammatory response through the damage equation and the inflammatory cell equation. These equations represent a subsystem within our model. Since perturbations in either the fibroblast or collagen deposition equations do not affect solutions to this system, the inflammatory system represents an isolated subsystem. Although the inflammatory system is isolated from the other equations in our model, it is particularly important because both fibroblast and collagen deposition equations are coupled to the inflammatory response. This makes the subsystem a key focal point in our model because small perturbations in inflammatory system may lead to unstable solutions to the overall system. Therefore, it is necessary to examine what conditions may lead to instabilities about homogeneous equilibrium points or steady state solutions associated with the inflammatory subsystem.

In a one dimensional rectangular geometry, the inflammatory system appears as

$$\frac{\partial m}{\partial t} = -\mu_{mn} m n \tag{3.1}$$

$$\frac{\partial n}{\partial t} = \frac{\partial}{\partial x}\left[D_n \frac{\partial n}{\partial x} - n\chi_n \frac{\partial m}{\partial x}\right] - \mu_{nm} m n \tag{3.2}$$

A homogeneous equilibrium point is a solution to this partial differential system that is constant in space and time. In other words, if $(\bar{m}, \bar{n})$ is a homogeneous equilibrium point, we may write

$$\frac{\partial \bar{m}}{\partial t} = \frac{\partial \bar{m}}{\partial x} = 0$$
$$\frac{\partial \bar{n}}{\partial t} = \frac{\partial \bar{n}}{\partial x} = 0$$

Applying these results to the inflammatory system produces

$$0 = -\mu_{mn}\bar{m}\bar{n} \tag{3.3}$$

$$0 = -\mu_{nm}\bar{m}\bar{n} \tag{3.4}$$

Examining Equations (3.3) and (3.4), we see that there are three possibilities for homogeneous equilibrium points. These include

1. $(\bar{m},\bar{n}) = (0,0)$,
2. $(\bar{m},\bar{n}) = (c,0)$,
3. $(\bar{m},\bar{n}) = (0,c)$.

In our wound repair model, we are particularly interested in solutions that are close the equilibrium point $(\bar{m},\bar{n}) = (0,0)$ since this represents a physical solution, which corresponds to the resolution of inflammation; however, we include the other two equilibrium points in our analysis for completeness.

To test the stability of our solutions, we consider perturbations away from a homogeneous equilibrium. We assume that these deviations are small in magnitude and that they are small with respect to their first and second derivatives. We represent these perturbations as follows

$$m(x,t) = \bar{m} + m'(x,t) \tag{3.5}$$

$$n(x,t) = \bar{n} + n'(x,t) \tag{3.6}$$

Substituting Equations (3.5) and (3.6) into the inflammatory system yields

$$\begin{aligned}
\frac{\partial}{\partial t}\left(\bar{m}+m'\right) &= -\mu_{mn}\left(\bar{n}+n'\right)\left(\bar{m}+m'\right) \\
\frac{\partial}{\partial t}\left(\bar{n}+n'\right) &= \frac{\partial}{\partial x}\left[D_n\frac{\partial}{\partial x}\left(\bar{n}+n'\right) - \left(\bar{n}+n'\right)\chi_n\frac{\partial}{\partial x}\left(\bar{m}+m'\right)\right] - \mu_{nm}\left(\bar{n}+n'\right)\left(\bar{m}+m'\right)
\end{aligned}$$

Since $\bar{n}\bar{m} = 0$ and $\frac{\partial \bar{n}}{\partial x} = \frac{\bar{m}}{\partial x} = 0$, we can simplify these expressions. Hence, these expressions become

$$\begin{aligned}
\frac{\partial m'}{\partial t} &= -\mu_{mn}\left(n'\bar{m} + \bar{n}m' + n'm'\right) \\
\frac{\partial n'}{\partial t} &= D_n\frac{\partial^2 n'}{\partial x^2} - \chi_n\frac{\partial n'}{\partial x}\frac{\partial m'}{\partial x} - \bar{n}\chi_n\frac{\partial^2 m'}{\partial x^2} - n'\chi_n\frac{\partial^2 m'}{\partial x^2} - \mu_{nm}\left(n'\bar{m} + \bar{n}m' + n'm'\right)
\end{aligned}$$

The terms $n'm'$, $\frac{\partial n'}{\partial x}\frac{\partial m'}{\partial x}$ and $n'\frac{\partial^2 m'}{\partial x^2}$ are quadratic in their perturbations or their derivatives. Consequently, these terms are smaller in magnitude than other terms. Hence, we drop them from our analysis, and the equations become

$$\frac{\partial m'}{\partial t} = -\mu_{mn}\left(n'\bar{m} + \bar{n}m'\right) \tag{3.7}$$

$$\frac{\partial n'}{\partial t} = D_n\frac{\partial^2 n'}{\partial x^2} - \bar{n}\chi_n\frac{\partial^2 m'}{\partial x^2} - \mu_{nm}\left(n'\bar{m} + \bar{n}m'\right). \tag{3.8}$$

Since these equations are now linear in n' and m', we examine solutions to the perturbation equations using the basis functions:

$$m'(x,t) = Ae^{\sigma t}\cos qx, \tag{3.9}$$

$$n'(x,t) = Be^{\sigma t}\cos qx. \tag{3.10}$$

In a more general setting, we could examine an infinite series of linear combinations of these functions; however, for simplicity, we merely examine this component since it is possible to construct more general solutions from these functions. Substituting Equations (3.9) and (3.10) into (3.7) and (3.8), respectively, we have

$$\begin{aligned}
\sigma Ae^{\sigma t}\cos qx &= -\mu_{mn}\left(\bar{m}B+\bar{n}A\right)e^{\sigma t}\cos qx \\
\sigma Be^{\sigma t}\cos qx &= \left[\bar{n}\chi q^2 A - D_n q^2 B - \mu_{nm}\left(\bar{m}B+\bar{n}A\right)\right]e^{\sigma t}\cos qx
\end{aligned}$$

Simplifying, we obtain

$$\begin{aligned}
&(\sigma+\mu_{mn}\bar{n})A+\mu_{mn}\bar{m}B=0 \\
&\left(\mu_{nm}-\chi_n q^2\right)\bar{n}A+\left(\sigma+D_n q^2+\mu_{nm}\bar{m}\right)B=0
\end{aligned}$$

If $A=B=0$, perturbations about the equilibrium condition are identically zero. This particular solution to the perturbation equations does not provide any insight into the stability about a particular equilibrium point. Therefore, in order to investigate nonzero perturbations, it is necessary to require that $A\neq 0$ and $B\neq 0$. This implies that

$$\det \begin{bmatrix} \sigma + \mu_{mn}\bar{n} & \mu_{mn}\bar{m} \\ \left(\mu_{nm} - \chi_n q^2\right)\bar{n} & \sigma + D_n q^2 + \mu_{nm}\bar{m} \end{bmatrix} = 0$$

Applying this result, we now investigate the stability about each homogeneous equilibrium point using our linear approximation.

Case 1:

If $(\bar{m}, \bar{n}) = (0, 0)$, then the coefficient matrix becomes

$$\begin{bmatrix} \sigma & 0 \\ 0 & \sigma + D_n q^2 \end{bmatrix}$$

The determinant of this matrix is

$$\sigma\left(\sigma + D_n q^2\right),$$

$\sigma(\sigma + D_n q^2) = 0$ implies $\sigma = 0$ or $\sigma = -q^2 D_n$. Since $D_n > 0$ and $q^2 > 0$, $\sigma \leq 0$. Since σ is not positive, we expect small perturbations to be bounded as $t \to \infty$ for this special case. Hence, solutions about the equilibrium point (0, 0) remain stable for any choice of constants.

Case 2:

Now, if $(\bar{m}, \bar{n}) = (c, 0)$ with $c > 0$, then the coefficient matrix becomes

$$\begin{bmatrix} \sigma & \mu_{mn} c \\ 0 & \sigma + D_n q^2 + \mu_{nm} c \end{bmatrix}.$$

Here, we compute the determinant as

$$\sigma\left(\sigma + D_n q^2 + \mu_{nm} c\right) = 0.$$

Thus, $\sigma = 0$ or $\sigma = -(q^2 D_n + \mu_{nm} c)$. Since $D_n,\ q^2,\ \mu_{nm} > 0$, we write $\sigma \leq 0$. Since σ is not positive, we expect small perturbations to be bounded as $t \to \infty$ for this special case. Hence, perturbations about the equilibrium point (c, 0) remain stable for any choice of constants.

Case 3:

If $(\bar{m}, \bar{n}) = (0, c)$ where $c > 0$, then the coefficient matrix becomes

$$\begin{bmatrix} \sigma + \mu_{mn} c & 0 \\ \left(\mu_{nm} - \chi_n q^2\right) c & \sigma + D_n q^2 \end{bmatrix}.$$

The determinant of this matrix is

$$\left(\sigma + \mu_{mn} c\right)\left(\sigma + D_n q^2\right),$$

which becomes

$$\sigma^2 + \left(\mu_{mn} c + D_n q^2\right)\sigma + \mu_{mn} c D_n q^2.$$

The determinant is identically zero. Therefore, the roots of this quadratic equation are given as

$$\sigma_{\pm} = \frac{-\left(\mu_{mn} c + D_n q^2\right) \pm \sqrt{\left(\mu_{mn} c + D_n q^2\right)^2 - 4\left(\mu_{mn} c D_n q^2\right)}}{2}$$

Rearranging terms yields

$$\sigma_{\pm} = \frac{-\left(\mu_{mn}c + D_n q^2\right) \pm \sqrt{\left(\mu_{mn}c - D_n q^2\right)^2}}{2}$$

This last results gives $\sigma_+ = -D_n q^2$ and $\sigma_- = -\mu_{mn}c$. Here $\sigma_+ < 0$ because $D_n > 0$ and $q^2 > 0$. For the later case, we have $\mu_{mn} > 0$, which implies $\sigma_- < 0$. Thus, we write $\sigma < 0$. Since σ is not positive, we expect small perturbations to be bounded as $t \to \infty$ for this special case. Hence, perturbations about the equilibrium point (0, c) remain stable for any choice of constants.

For cases (1) and (2), it is important to note that the analysis as described above is valid only for the special case. In a more general context, we can not draw the same conclusions for either of these cases when $\sigma = 0$. This is because an infinite sum of cosines (i.e. a Fourier cosine series) could produce a valid solution to the perturbation equations. This solution may be unbounded in finite time for some $x \in D_n$ yielding an unstable perturbation. We leave this investigation and the analysis of the inflammatory system in a cylindrical geometry as important topics of another investigation.

Problem Domain

Implantable models provide experimentally controlled environments which aid in the development of mathematical models. Our goal is to create a mathematical system which describes aspects of wound repair within the framework of the synthetic implant. Consequently, we constrict the domain of our mathematical system so that it conforms to the geometry of the implant. This is illustrated by Figure 4.1.

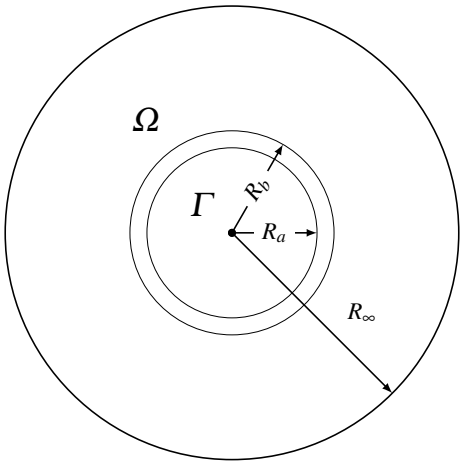

Figure 4.1: View along the axis of symmetry of the implant

Figure 4.1 depicts the hypothetical domain of the implantable wound repair model. Here, R_a and R_b represents the inner and outer radius of the implant, respectively. R_∞ depicts the outer regions of the wound, not the wound boundary, where $R_\infty >> R_b$. For the case of a PVA or ePTFE sponge, the inner annulus does not exist, and the radius of the implant can be solely described as $r = R_b$. For the scenario depicted in Figure 4.1, Ω represents the region of tissue damage, and Γ represents the inner region of the implant. For simplicity, we shall

assume that these regions are the same with regard to the damage marker. In other words, we assume that damage extends into the implant, and it attains its maximum value at $r = 0$.

We must make a cautionary note regarding the problem domain illustrated in Figure 4.1. This figure is misleading in the sense that one might draw the conclusion that Ω represents the wound boundary. This is not the intention. Here, Ω defines the problem domain. In this work, the wound is indirectly represented by the damage marker $m(\vec{r},t)$. The initial damage is given by the initial condition $m(\vec{r},0)$, which we shall discuss in the next section.

Rather than directly apply the scenario depicted in Figure 4.1, we wish to establish a baseline model within the confines of the implantable system. Hence, we assume the cylindrical approximation illustrated in Figure 4.2. This figure illustrates the problem domain within the confines of the implant. Here, we have adopted the PVA or ePTFE sponge structure. The geometry in Figure 4.2 has tremendous benefits in that it simplifies our system of partial differential equations. The symmetry of the implantable system reduces our equations to two independent variables, namely time and space.

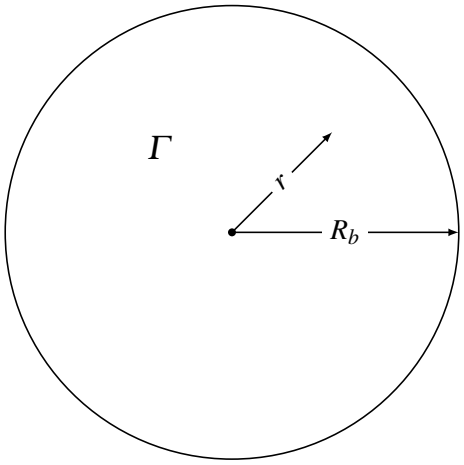

Figure 4.2: Problem domain without implantable system

In Figure 4.2, R_b is a constant that represents the boundary of the implant and r is a dependent variable such that $0 < r < R_b$. The domain, Γ, is defined as the set $\{(x,y) : \sqrt{x^2+y^2} \leq R_b\}$.

From symmetry, we expect $\frac{\partial u}{\partial \theta} = 0$ and $\frac{\partial u}{\partial z} = 0$, where u is a place holder for m, n, f and c. This condition reduces both the gradient and the divergence operators as follows

$$\begin{aligned} \nabla u &= \hat{r}\frac{\partial u}{\partial r} && (4.1) \\ \nabla \cdot \vec{u} &= \frac{1}{r}\frac{\partial}{\partial r}(r u_r). && (4.2) \end{aligned}$$

In Equation (4.1), we have $u : \mathbb{R}^3 \to \mathbb{R}$. In other words, u is a scalar function. In Equation (4.2), $\vec{u} : \mathbb{R}^3 \to \mathbb{R}^3$ is a vector-valued function, and u_r, a scalar function, is the component of $\vec{u}$ in the radial direction. Consequently, our system reduces to a set of time dependent equations with one spatial component, which are given as follows

$$\begin{aligned} \frac{\partial m}{\partial t} &= -\mu_{mn} m n, && (4.3) \\ \frac{\partial n}{\partial t} &= \frac{1}{r}\frac{\partial}{\partial r}\left[D_n r \frac{\partial n}{\partial r} - n\chi_n r \frac{\partial m}{\partial r}\right] - \mu_{nm} m n, && (4.4) \\ \frac{\partial f}{\partial t} &= \frac{1}{r}\frac{\partial}{\partial r}\left[D_f r \frac{\partial f}{\partial r} - f\chi_f c r \frac{\partial f}{\partial r}\right] + k_f f\left(2 - \frac{f}{F_0}\right) - \mu_f f, && (4.5) \\ \frac{\partial c}{\partial t} &= k_c f (C_0 - c) - \mu_{cn} c n, && (4.6) \end{aligned}$$

where we now have functions $m(r,t)$, $n(r,t)$, $f(r,t)$ and $c(r,t)$ rather than $m(\vec{x},t)$, $n(\vec{x},t)$, $f(\vec{x},t)$ and $c(\vec{x},t)$, respectively.

4.1 Boundary Conditions

Here we discuss the boundary conditions of our PDE system. At the left end point, $r = 0$, we impose the following symmetry condition for all equations.

$$\frac{\partial m(0,t)}{\partial r} = \frac{\partial n(0,t)}{\partial r} = \frac{\partial f(0,t)}{\partial r} = \frac{\partial c(0,t)}{\partial r} = 0$$

At the right end point, $r = R_b$, the boundary conditions for each equation are quite different from one another. For the damage equation, we impose the same type of boundary condition, but the rationale is different. Since the damage marker does not diffuse throughout the wound, we impose the condition

$$\frac{\partial m(R_b,t)}{\partial r} = 0.$$

This condition represents a zero flow condition due to the fixed nature of the tissue damage. The right boundary condition for the inflammatory cell equation is difficult to model. Inflammatory cells are produced in the spleen, and they are activated thorough transport mechanisms via blood stream, which are beyond the the scope of the model's domain. In our model, we do not model cytokines directly. Rather, we assume that gradient's of PDGF and TGF-β are proportional to the species that release them, namely inflammatory and fibroblast cells. To arrive at a suitable boundary condition, we must consider several factors. First, we consider the pool of resting inflammatory cells to be very large and their production rate to be under a quasi-steady state condition. Also, we assume the the activation and transport of inflammatory cells to be very fast as compared to the time scale of wound repair. Hence, in this work, we assume that at the right boundary the injection of inflammatory cells into the wound is proportional to the quantity of damage at the boundary. We express this by the following relationship

$$n(R_b,t) = \kappa_m m(R_b,t)$$

Another suitable choice of boundary conditions would be to set the density of inflammatory cells at the boundary proportional to the gradient of damage at the boundary. In other words

$$n(R_b,t) = \kappa \frac{\partial m(R_b,t)}{\partial x}.$$

We will explore this option in future studies. The damage caused by the initial infraction dissipates as one approaches the edge of the wound. Therefore, fibroblasts should approach their nominal levels as $r \to R_b$. For this reason, we approximate the density of fibroblasts at right boundary point to be equivalent to the nominal density of fibroblasts in healthy tissue. Thus, the right boundary condition becomes

$$f(R_b,t) = F_0$$

Since new granulation tissue and collagen deposited by fibroblasts is fixed, we impose the same no flow condition as we did with right boundary point of the initial damage. Thus, we have following boundary condition for new tissue deposition:

$$\frac{\partial c(R_b,t)}{\partial t} = 0,$$

at the right boundary point.

4.2 Initial Conditions

The initial conditions of our PDE system account for the state of the variables at the onset of injury. We assume that the profile of the initial damage marker is Gaussian, and it achieves a maximum at the center of the wound or implant. The initial condition for damage is as follows

$$m(r,0) = M_0 e^{-C_m r^2}.$$

Here M_0 is the maximum density of damage, C_m is the Gaussian decay constant. For our other two equations, we assume that their values at the boundary slough off into the wound. We use exponential forms to express this phenomena. Here, we have

$$\begin{aligned} n(r,0) &= n(R_b,0)e^{-C_n(R_b-r)} \\ f(r,0) &= F_0 e^{-C_f(R_b-r)}. \end{aligned}$$

These equations represents the initial conditions for inflammatory and fibroblast cells, respectively. For the former equation, $n(R_b,t)$ is the boundary condition for inflammatory cells at $t = 0$, and C_n is the decay constant. The latter equation, which represents the initial condition for fibroblasts, has a very similar form. Here, F_0 is the density of fibroblasts in healthy tissue, and C_f is the decay constant for fibroblast density.

Since C_0 represents the density of healthy tissue, then the initial wound profile, $c(r,0)$, may be represented as c(r,0) = C_0 - m(r,0), where c is the profile of collagen in the wound. However, we must be careful how we treat the time evolution of such an equation in our model because the removal of nonfunctional matrix is distinct from the deposition of a new collagen matrix. This leads to the following initial condition for the initial undamaged

collagen profile.

$$c(r,0) = C_0 - M_0 e^{-C_m r^2}.$$

Simulation & Results

5.1 Modeling Biological Systems

One of the difficulties with mathematically modeling any biological system is the procurement of parameters which describe the fundamental properties of the system. The issue of biological variability and complexity make it difficult for biologists to make quantitative measurements of these parameters in the same way a physicist might measure a fundamental constant of nature. Consequently, there is currently very little information with regard to the fundamental properties associated with wound healing. For this reason, we attempt to elucidate values for coefficients in our mathematical system from simulations performed with our PDE model. Before we can use our model in this way, we first must identify a set of values that characterize the behavior of a given unknown during the repair process. In addition, we must also define criteria so that we can arbitrarily evaluate how well a given solution predicts its characteristic information.

Characteristic Values

Since our system of equations accounts for the time rate of change of a set variables, it is natural to model to characteristic values that are associated with key time periods associated with repair. For example, characteristic values, which describe the period it takes an unknown to reach its local maximum or steady state, are ideal for our purposes. An acute dermal wound presents a degree of difficulty in this respect because the rate of change for a given unknown is dependent on many factors. For example, the rate of healing is dependent

on parameters such as tissue oxygenation, pathogen level, and wound size. Because these factors may be inconsistent among studies, rates of development may be reported differently. Therefore, we attempt to pick a set of characteristic values that are uniform with an acute dermal wound which heals of its own accord. If these values should changed based upon different objectives, we should be able to fit our model to a different set of characteristics. That is our PDE model may be tailored to a new set of characteristic values. What is important is that our model predicts the general progression of events associated with our unknowns based upon the defining characteristics that we choose.

For a given unknown, we assign three characteristic time periods. These refer to a given unknown's behavior during the repair process. We define each of these characteristic intervals as follows

1. initial response time, $\Delta t_{in} = t_{in} - t_0$: the time period in which an unknown begins to initially accumulate at a given location in the wound starting from the onset of injury or implantation,

2. peak response time, $\Delta t_{max} = t_{max} - t_0$: the time period in which an unknown attains its maximum value at a given location in the wound starting from the onset of injury or implantation,

3. equilibrium or steady state response time, $\Delta t_{fn} = t_{fn} - t_0$: the time period in which an unknown approaches or becomes arbitrarily close to its steady state value at a given location in the wound starting from the onset of injury or implantation.

Here, t_0 represents the time of injury or implantation. Table 5.1 illustrates our choice of characteristic values for each unknown in our model. We constructed this table based upon information obtained from our literature search. We discussed many of these characteristics in Section 1.1. Table 5.1 summarizes this information for convenience. All information

displayed in this table is reported in days. In Table 5.1, we have cross referenced each of the characteristic values with the source from which they were obtained.

Unknown	Δt_{in} $(days)$	Δt_{max} $(days)$	Δt_{eq} $(days)$
Neutrophils	1 [1], [5], [6]	$1-2$ [5], [9]	3 [5], [9]
Macrophages	2 [1], [5]	$2-7$ [2], [5]	7 [2], [3], [5]
Fibroblasts	$2-3$ [11],[12]	7 [5], [12]	14 [5]
Collagen	$7-10$ [37]	$7-10$ [12]	$14-21$ [2], [5], [11]

Table 5.1: Characteristic intervals associated with repair.

Using the data presented Table 5.1, we can construct a notional time line which depicts the natural progression associated with each of our unknowns during repair. The figure illustrates this for neutrophils, macrophages, fibroblasts and collagen deposition. In Figure 5.1, all curves have been drawn to reflect their respective values tabulated in Table 5.1. The immune response reflects the sum of neutrophil and macrophage activity. We assume that active neutrophils and macrophages approach a steady state value of zero. This is because once the inflammatory phase comes to an end, these cells are no longer required to remove debris from the wound. Figure 5.1 also outlines characteristics associated with fibroblast infiltration and collagen deposition. Since it has been reported that fibroblasts begin apoptosis once collagen deposition levels off [11], we assume that fibroblasts and collagen reach their equilibrium points congruently.

Figure 5.1 provides a valuable check when examining potential solutions that stem from our system of equations; however, we use the information presented in Table 5.1 to fit the parameters of our model. To do this, we carry out a number of simulations until we

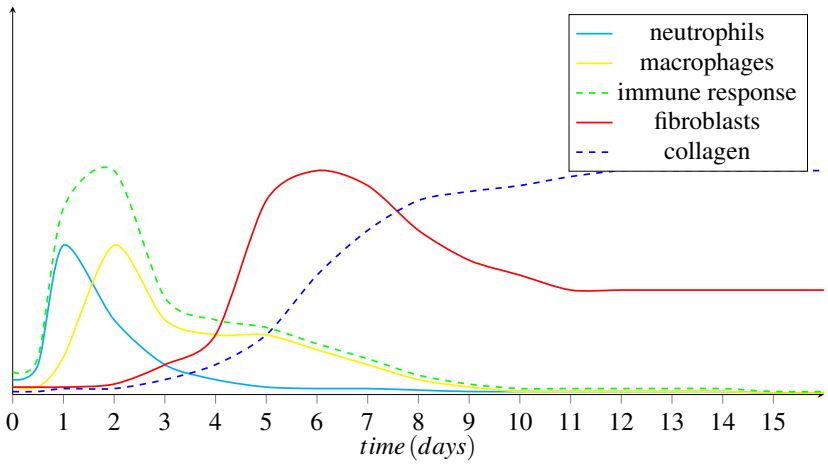

Figure 5.1: Notional time line for events involved in repair.

are able to approximate the information reported in Table 5.1 with a numerical solution obtained from our PDE model. The results of this process are presented in Section 5.3. Once we fit our model with a suitable set of parameters, we validate the model and numerical solution with data obtained from ePTFE implants. We discuss these results in Section 5.5.

Evaluation Criteria

Once we have obtained a solution that presents a reasonable fit to the data in Table 5.1, it is important to evaluate the solution in mathematical terms. This can be easily accomplished by computing the relative error between characteristic values reported in Table 5.1 and their corresponding values produced from a given solution. For certain characteristic values such as Δt_{max}, this is not an issue; however, the continuous nature associated with our solutions present difficulties in determining characteristic values such as Δt_{in} and Δt_{fn}. This is because concepts such as "closeness" are subjective. For this reason, we defined the following methodology to make consistent evaluations for these characteristic values.

Consider an unknown, $u : D \times I \to \mathbb{R}$ where $I = [t_0, t_f]$ and $D = [0,1]$. We define the following sets

$$I_{in} = \{t \in I : 0 < u(r = R, t) - u(r = R, t = t_0) = K\},$$
$$I_{fn} = \{t \in I : \left|u(r = R, t) - u(r = R, t = t_f)\right| = K\},$$

where $r \in D$, $t \in I$ and $K > 0$ is a positive constant, which we set arbitrarily for a particular investigation. Here, t_0 retains its previous definition, t_f represents an arbitrary time such that $t_f > t_0$ and R is a distinct point in the wound domain. Usually, $t_0 = 0$. If I_{in} or I_{fn} is an empty set, then we must reevaluate our choice for K. Now, using these sets, we define the following characteristic times associated with a given solution

$$t_{in} = \min I_{in}, \tag{5.1}$$
$$t_{max} = \arg\max_{t \in I} u(r = R, t), \tag{5.2}$$
$$t_{fn} = \max I_{fn}. \tag{5.3}$$

Here, $\arg\max u(t)$, where $t \in I$, represents the argument of u where u achieves its relative maximum. Computation of Δt_{in}, Δt_{max} and Δt_{fn} follow directly from definitions 5.1, 5.2 and 5.3, respectively. For our analysis, we let $K = 0.1$. As far as our choice of R is concerned, the wound center provides an optimum candidate for our evaluation criteria. This is because the initial value for each unknown at this point is reasonably small (i.e. close to zero). Hence, we set $R = 0$ for the verification of our solution.

5.2 Quasi-Dimensionless System

Before we fit the parameters associated with our model, we transition our system to a quasi-dimensionless system, and we normalize each dependent variable using the fundamental parameters of the model. The rationale behind this endeavor is two-fold. First, this reduces the total number of parameters that are necessary to describe our wound repair system. Consequently, this reduces the number of degrees of freedom in our model and cuts down on the number of simulations that must be preformed in order to deduce these values. Second, removing these parameters accounts for a degree of biological variability that occurs between individuals. Fundamental parameters such as M_0, F_0, C_O and R_b describe the state of a particular system. These values may change based upon the degree of damage or the size of the wound in a particular study. In addition, the nominal level of fibroblasts or collagen matrix may vary based upon the test subject who may be a healthy individual or who may present some pathological state.

In this work, we used the transformation $\bar{r} = r/R_b$ and $\bar{t} = t$ and then normalize the wound repair system using the terms M_0, N_a, F_0 and C_0. Here N_a represents the concentration of activated inflammatory cells in a normal individual. The differential operators of our system become

$$\frac{\partial}{\partial t} = \frac{\partial}{\partial \bar{t}}, \tag{5.4}$$

$$\frac{\partial}{\partial r} = \frac{1}{R_b}\frac{\partial}{\partial \bar{r}}. \tag{5.5}$$

Applying these operators to our system of equations, normalizing and then collecting terms yields

$$\frac{\partial \bar{m}}{\partial \bar{t}} = -\mu^*_{mn}\bar{m}\bar{n}, \tag{5.6}$$

$$\frac{\partial \bar{n}}{\partial \bar{t}} = \frac{1}{\bar{r}}\frac{\partial}{\partial \bar{r}}\left[D^*_n\bar{r}\frac{\partial \bar{n}}{\partial \bar{r}} - \bar{n}\chi^*_n\bar{r}\frac{\partial \bar{m}}{\partial \bar{r}}\right] - \mu^*_{nm}\bar{m}\bar{n}, \tag{5.7}$$

$$\frac{\partial \bar{f}}{\partial \bar{t}} = \frac{1}{\bar{r}}\frac{\partial}{\partial \bar{r}}\left[D^*_f\bar{r}\frac{\partial \bar{f}}{\partial \bar{r}} - \bar{f}\chi^*_f\bar{r}\frac{\partial \bar{n}}{\partial \bar{r}}\right] + k_f\bar{f}\left(2-\bar{f}\right) - \mu_f\bar{f}, \tag{5.8}$$

$$\frac{\partial \bar{c}}{\partial \bar{t}} = k^*_c\bar{f}(1-\bar{c}) - \mu^*_{cn}\bar{c}\bar{n}, \tag{5.9}$$

where $\bar{m}$, $\bar{n}$, $\bar{c}$ and $\bar{f}$ are now expressed as dimensionless terms. The parameters of the system are redefined as

$$\mu^*_{mn} = \mu_{mn}N_a,$$

$$D^*_n = D_n/R_b^2,$$

$$\chi^*_n = M_0\chi_n/R_b^2,$$

$$\mu^*_{nm} = \mu_{nm}M_0,$$

$$D^*_f = D_f/R_b^2,$$

$$\chi^*_f = N_a\chi_f/R_b^2,$$

$$k^*_c = k_cF_0,$$

$$\mu^*_{cn} = \mu_{cn}N_a.$$

Here, each parameter is now expressed in the units of $time^{-1}$. The coefficients k_f and μ_f remain unaffected by our transformation and normalization. Applying the same operations to our boundary and initial conditions yields

$$\frac{\partial \bar{m}(0,t)}{\partial \bar{r}} = \frac{\partial \bar{n}(0,t)}{\partial \bar{r}} = \frac{\partial \bar{f}(0,t)}{\partial \bar{r}} = \frac{\partial \bar{c}(0,t)}{\partial \bar{r}} = 0,$$
$$\frac{\partial \bar{m}(1,t)}{\partial \bar{r}} = \frac{\partial \bar{c}(1,t)}{\partial \bar{r}} = 0,$$
$$\bar{n}(1,t) = \kappa_m^* \bar{m}(1,t),$$
$$\bar{f}(1,t) = 1$$

for boundary conditions, and

$$\bar{m}(\bar{r},0) = e^{-C_m^* \bar{r}^2},$$
$$\bar{n}(\bar{r},0) = \bar{m}(1,0) e^{-C_n^*(1-\bar{r})},$$
$$\bar{f}(\bar{r},0) = e^{-C_f^*(1-\bar{r})},$$
$$\bar{c}(\bar{r},0) = 1 - \bar{m}(\bar{r},0)$$

for the initial conditions. For these cases, parameters are redefined as follows

$$\kappa_m^* = \kappa_m M_0 / N_a,$$
$$C_m^* = C_m R_b^2,$$
$$C_n^* = C_n R_b,$$
$$C_f^* = C_f R_b,$$

5.3 Parameter Selection

Simulations were perform using a combination of PDEONE (algorithm 494) [38], [39] and the PDEPE solver provided by MATLAB. Algorithm 494 is an interface routine that uses the numerical method of lines for solving a system of nonlinear partial differential equations. The method essentially discretizes a spatial variable(s) of a time dependent partial differential equation forming an approximating system of ordinary differential equations (ODEs). Numerical techniques for solving systems of ODEs are then used to solve the resulting system of equations and thus the original problem. The algorithm handles nonlinear systems of equations of the form

$$\frac{\partial u_k}{\partial t} = f_k\left(t, x, \vec{u}, \frac{\partial \vec{u}}{\partial x}, \frac{1}{x^n}\frac{\partial}{\partial x}x^n\left(\vec{D}_k \cdot \frac{\partial \vec{u}}{\partial x}\right)\right),$$

with boundary conditions

$$\alpha_k u_k + \beta_k \frac{\partial u_k}{\partial x} = \gamma_k,$$

and initial conditions

$$u_k(t_0, x) = \phi_k(x).$$

Here $x \in [a,b]$, $k \in \mathbb{N}$, and n is 0, 1 or 2 depending on whether the problem is in Cartesian, cylindrical or spherical coordinates, respectively. If $\beta_k \neq 0$, then α_k, β_k and γ_k may be functions of t and $\vec{u}$. We used the Runge-Kutta Chebychev solver, RKC, to solve the resulting underlying system of ODEs produced by algorithm 494. Simulations with PDEONE were carried out in the Octave computational environment. We used a C++ wrapper that integrates the PDEONE solver with the Octave framework [40]. The PDEPE solver provided by MATLAB was primarily used as a check for specific solutions. In addition, MATLAB

functionality was also used for processing solution results and plotting graphs. In our analysis, all simulations were performed with a spatial step size of 0.05 and a temporal step size of 0.001.

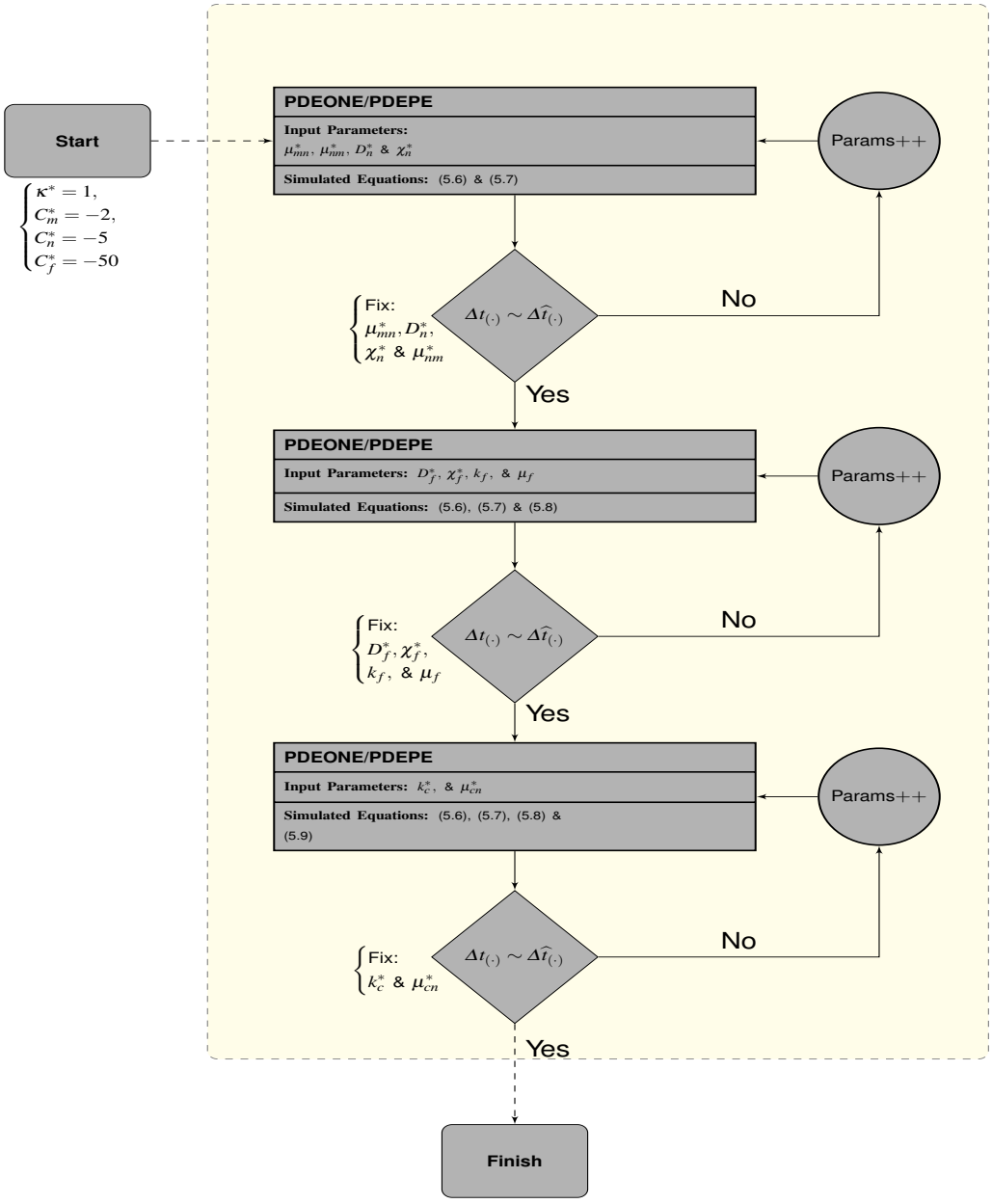

Figure 5.2: Schema for fitting parameters of the wound repair model

In order to reduce the total number of simulations, we implemented the schema shown

in Figure 5.2. Here, we exploited the structure present in our system of equations. As initial inputs, we set κ^*, C_n^*, C_m^* and C_f^* to 1, -2, -5 and -50, respectively. Because the inflammatory system represents an isolated subsystem within our model, we initially preformed simulations solely using this system to obtained an initial set of candidates for parameter selection. Here, we let the parameters μ_{mn}^*, D_n^*, χ_n^* and μ_{nm}^* vary over several simulations. Simulations were performed using either PDEONE or PDEPE. For a given simulation, parameter values were fixed. Solutions obtained from a simulation were qualitatively screened for their goodness of fit. This is indicated by the decision point $\Delta t_{(\cdot)} \sim \Delta\widehat{t}_{(\cdot)}$ in Figure 5.2. Here, $\Delta t_{(\cdot)}$ and $\Delta\widehat{t}_{(\cdot)}$ represent characteristic values obtained from Table 5.1 and a given solution, respectively. If a set of parameters provided a poor fit, they were discarded and a new set was provided. This is indicated by the branch label Params++ in Figure 5.2. After simulations completed, we fixed the coefficients of the inflammatory subsystem by selecting an appropriate solution from a set of potential candidates whose criteria was in reasonable agreement with the characteristic values reported in Table 5.1. This cycle was repeated twice more, first, with the fibroblast equation, and again, with the collagen equation. Since the fibroblast equation only depends upon inflammatory equation, this equation was incorporated into the inflammatory subsystem to form a three equation model, and the parameters obtained via simulations with the inflammatory subsystem were used as input to this new subsystem. Simulations were then performed with the three equation model to deduce an optimal set of parameters for the fibroblast equation. Finally, we implemented this procedure once more to finalize a complete set of coefficients for our wound repair model. Once the entire methodology illustrated in Figure 5.2 was completed, we arrived at the set of parameters shown in Table 5.2.

Figure 5.3(a) compares the solution obtained from parameters displayed in Table 5.2 with the notional time line we constructed in Figure 5.1. We display both figures side by side for convenience. Figure 5.3(a) plots the normalized density of inflammatory cells, fibroblasts

Parameter	Definition	Value ($days^{-1}$)
μ^*_{mn}	*Damaged tissue consumption rate*	0.50
D^*_n	*Activated inflammatory cell diffusion constant*	0.05
χ^*_n	*Activated inflammatory cell chemotactic constant*	0.70
μ^*_{nm}	*Activated inflammatory cell death rate from phagocytosis*	0.10
D^*_f	*Fibroblast diffusion constant*	0.03
χ^*_f	*Fibroblast chemotactic constant*	0.10
k_f	*Fibroblast growth rate*	0.30
μ_f	*Fibroblast death rate*	0.30
k^*_c	*Collagen deposition rate*	0.30
μ^*_{cn}	*Collagen damage rate*	0.10

Table 5.2: Model coefficient values

and collagen obtained from our simulation. This figure shows how each of the unknowns in our model evolve as time progresses at the wound center, $\bar{r} = 0$. Figure 5.3(b) illustrates the notional model or time line from Figure 5.2. The response curves obtained from our model predict the general progression of their respective notional curve. In Figure 5.3(a), the inflammatory cell curve, shown in green, corresponds to the inflammatory response, red dashed line in Figure 5.3(b).

Given the solution curves shown in Figure 5.3(a), we now apply a more rigorous comparison. Below, we compute the characteristic values associated with each unknown using data obtained from the simulation. Again, we set $K = 0.1$ for these computations. For inflammatory cells, we have

$$\bar{n}_{\Delta t_{in}} = t_{in} - 0 = \min I_{in} = \min\{0.4, 19.1\} = 0.4,$$

$$\bar{n}_{\Delta t_{max}} = t_{max} - 0 = \max \arg_{t \in I} \bar{n}(\bar{r} = 0, t) = 1.5,$$

$$\bar{n}_{\Delta t_{fn}} = t_{in} - 0 = \max I_{fn} = \max\{0.8, 13.4\} = 13.4.$$

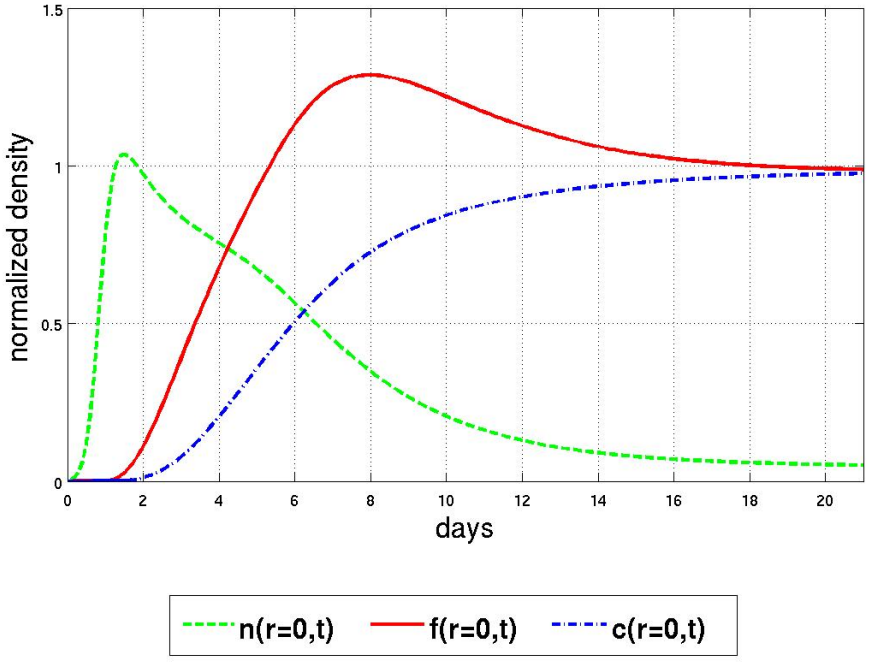

(a) Simulated wound repair time line at $\bar{r} = 0$

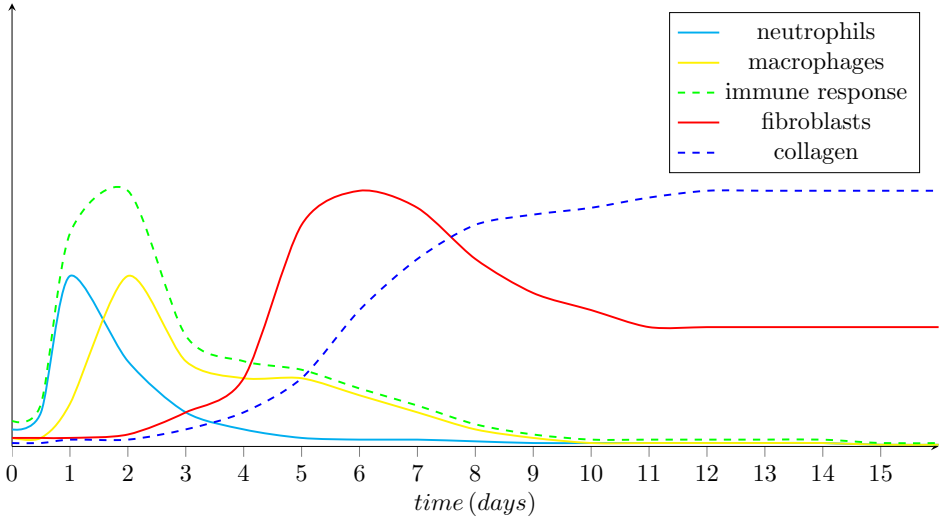

(b) Hypothetical wound repair time line

Figure 5.3: Simulated versus hypothetical time lines

For fibroblasts, our evaluation criteria yields

$$\bar{f}_{\Delta t_{in}} = t_{in} - 0 = \min I_{in} = \min\{1.9\} = 0.4,$$
$$\bar{f}_{\Delta t_{max}} = t_{max} - 0 = \max \arg_{t \in I} \bar{f}(\bar{r} = 0, t) = 8,$$
$$\bar{f}_{\Delta t_{fn}} = t_{in} - 0 = \max I_{fn} = \max\{5.1, 5.8, 12.8\} = 12.8.$$

Finally, for collagen deposition, we have

$$\bar{c}_{\Delta t_{in}} = t_{in} - 0 = \min I_{in} = \min\{3.2\} = 3.2,$$
$$\bar{c}_{\Delta t_{max}} = t_{max} - 0 = \max \arg_{t \in I} \bar{c}(\bar{r} = 0, t) = 21,$$
$$\bar{c}_{\Delta t_{fn}} = t_{in} - 0 = \max I_{fn} = \max\{12\} = 12.$$

These values are summarized in Table 5.3. Examination of this data shows that the characteristic time periods computed for inflammatory cells, fibroblasts and collagen show reasonable agreement with their respective values recorded in Table 5.1, and consequently, their values reported in the literature on wound healing.

$\bar{u}(\bar{r} = 0, t)$	Δt_{in} $(days)$	Δt_{max} $(days)$	Δt_{fn} $(days)$
$\bar{n}(\bar{r} = 0, t)$	0.4	1.5	13.4
$\bar{f}(\bar{r} = 0, t)$	1.9	8	12.8
$\bar{c}(\bar{r} = 0, t)$	3.2	21	12

Table 5.3: Characteristic intervals obtained from the numerical solution.

Several comments are in order regarding the simulation results in Figure 5.3(a) and characteristic values reported in Table 5.1 and 5.3. To begin with, consider the inflammatory response curve, $\bar{n}(0,t)$. In our model, this response represents the combination of neutrophils and macrophages. Neutrophils, typically, mount the initial immune response. This occurs within the first few hours directly following injury [1]. Our model reflects this datum. We computed an initial period of inflammatory cell infiltration, $\bar{n}_{\Delta t_{in}}$, to be 9.6 hours or 0.4 days. Neutrophil levels peak approximately 48 hours after injury and their levels fall to nominal values within 72 hours [5], [9]. During the former period, macrophages begin to accumulate at the wound site [1], [5]. From our literature review, it is not clear when these immune cells attain their maximum value; however, since it has been reported that macrophages begin to accumulate in the wound by day 2 and resolve by day 7 [2], [5], we assume that that they attain there maximum value between these extremes. Our model indicates that inflammatory cells have a peak response, $\bar{n}_{\Delta t_{max}}$, of 1.5 days. Since we do not distinguish between neutrophils and macrophages in our model, the values that we computed for the initial and peak response periods for inflammatory cells seem reasonable.

Although the transient immune response in our PDE model is in accord with the data tabulated in Table 5.1, its steady state response does not fit to the characteristic data tabulated in Table 5.1. This observation represents the largest point of discrepancy between values produced by our model and those in Table 5.1. As previously stated, the inflammatory response typically resolves itself within a 7 day period [2], [3], [5]. The inflammatory curve in figure 5.3 indicates that substantial levels of these cells still remain in the wound at this time. In this regard, inflammatory cell values are approximately 50% of their maximum value. In our model, the immune response has a steady state response time, $\bar{n}_{\Delta t_{fn}}$, of 13.4 days. Thus, the inflammatory phase predicted by our model appears appreciable longer than that reported in the literature.

In contrast, the characteristic time periods computed from fibroblast, $\bar{f}(0,t)$, and collagen

deposition, $\bar{c}(0,t)$, response curves compare more favorably with their counterparts in Table 5.1. For instance, fibroblast results from our model are in good agreement with their characteristic values. Our computation indicates these cells have an initial response period, $\bar{f}_{\Delta t_{in}}$, of 1.9 days. The respective values obtain from the literature were 2-3 days [11], [12]. In addition, results also show that fibroblasts have a maximum response time, $\bar{f}_{\Delta t_{max}}$, of 8 days in our model. Table 5.1 reports this value to be approximately 7 days [5], [11]. Finally, we computed a steady state response, $\bar{f}_{\Delta t_{fn}}$, for fibroblasts to be 12.8 days, which is in reasonable agreement with the value obtained from Lorenz et al. [5].

Lastly, Table 5.1 reports that collagen deposition reaches its maximum 14-21 following injury [2], [5], [12]. This is a critical point in wound repair because the fibroblast response is highly coupled with collagen deposition. During the final stages of the proliferation phase, fibroblasts under go apoptosis, and their numbers enter an equilibrium between new fibroblast production and those that undergo cell death [11]. At this point, we assumed that collagen approaches its homogeneous steady state. We computed a steady state response time, $\bar{c}_{\Delta t_{fn}}$, of 12 days. This period indicates that the wound has finished with proliferation and started the remodeling phase.

5.4 Simulation Results

We now discuss the overall simulation results in the context of a wound which undergoes repair. Figures 5.4, 5.5 and 5.6 display the numerical results when these parameters are used to simulate wound repair within the geometric constraints of a synthetic implant. In Figure 5.4(a), 5.5(a) and 5.6, we plot the normalized density of an unknown against the radius of the wound domain. Here, $0 \leq \bar{r} \leq 1$, where 0 is the wound center and 1 is the outer edge of the implant. The subplots shown in each figure represent a specific snapshot in time. As an alternative, we provide a 3-dimensional view for each variable as repair

proceeds. These are illustrated in Figures 5.4(b) and 5.5(b). These figures were generated by performing a 3-dimensional rotation of their respective 1-dimensional plots along the axis of symmetry. Snapshots for Figures 5.4(b) and 5.5(b) are provided for each time point illustrated in Figures 5.4(a)and 5.5(b), respectively. Each figure separates the solution into three distinct periods to illustrate the evolution of each variable described in our model. For convenience, we refer to these periods as the initial, intermediate and steady state phases. The initial phase covers the first 24 hours after injury. This period primarily captures the initial transient response of each unknown, particularly the inflammatory response. By comparison, the intermediate phase covers the first two weeks after injury. During this phase, unknowns still behave transiently; however, the proliferation response, rather than the inflammatory response, becomes the dominant response. Finally, the steady state phase includes time points where the solution converges on its homogeneous steady state solution, or repaired state.

Figure 5.4 shows the response of the system within the initial 24 hours directly following injury. Specifically, this plot displays the response for 0, 7.2, 14.4, 16.8, 19.2 and 24 hours after injury. The first plot in the upper left hand corner of Figure 5.4 shows the initial conditions at the time of injury. In this plot, damaged tissue, $\bar{m}(\bar{r},t)$, increases as we approach the center of the wound where we assume the injury occurred. The normalized density of inflammatory cells and fibroblasts, $\bar{n}(\bar{r},t)$ and $\bar{f}(\bar{r},t)$ respectively, exponentially drop off as we move inward from the edge of the wound, $\bar{r}=1$, into the region where tissue damage increases. For inflammatory cells, the value at the wound boundary represents the level of activated inflammatory cells which respond to the intensity of damage at the boundary. This is our boundary condition $\bar{n}(\bar{r}=1,t)=\kappa^*\bar{m}(\bar{r}=1,t)$. In the case of fibroblasts, their values at the boundary represent their nominal levels in health tissue. Their levels fall off exponentially due to the initial damage as $\bar{r}\to 0$. The profile of undamaged collagen, $\bar{c}(\bar{r},t)$, is simply the complement of the damaged tissue profile.

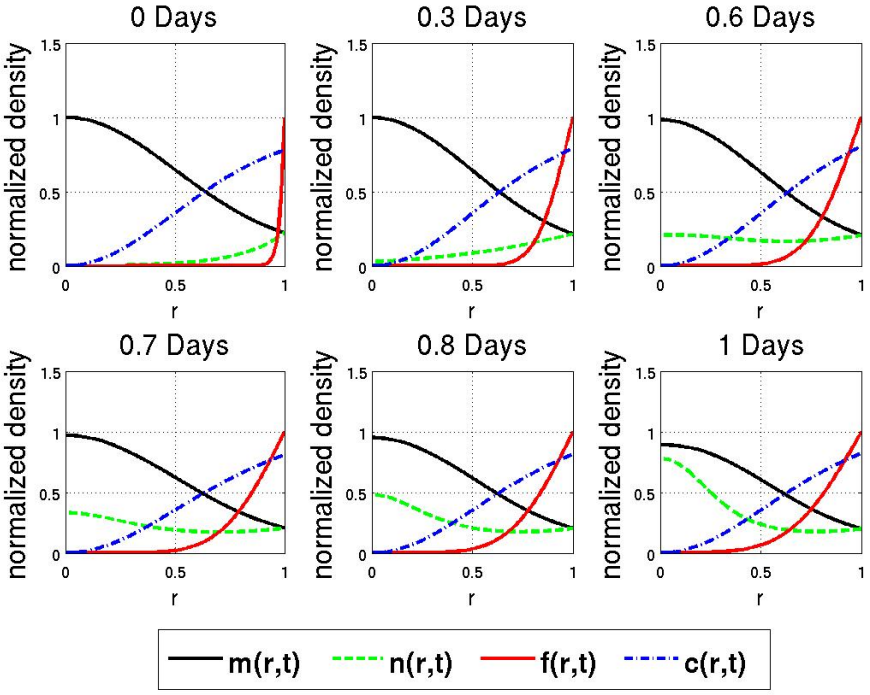

(a) 1-Dimensional plots along radial coordinate

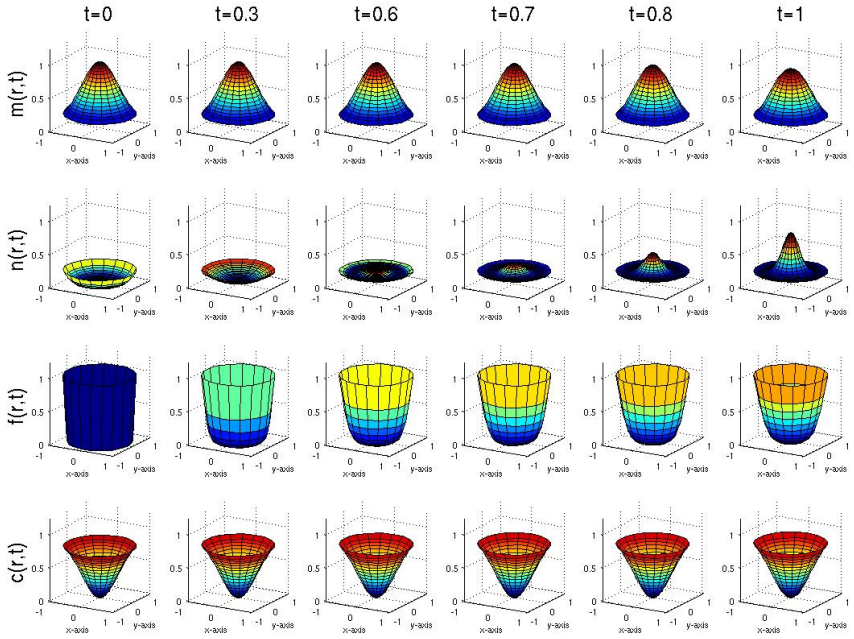

(b) 3-Dimensional rotational plots about axis of symmetry

Figure 5.4: Simulation of first 24 hours post-injury

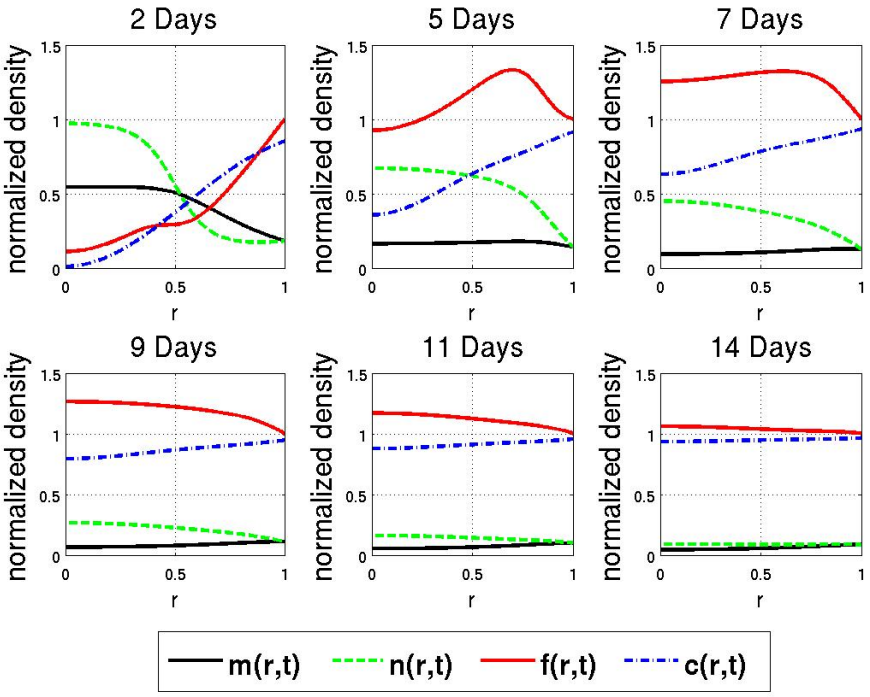

(a) 1-Dimensional plots along radial coordinate

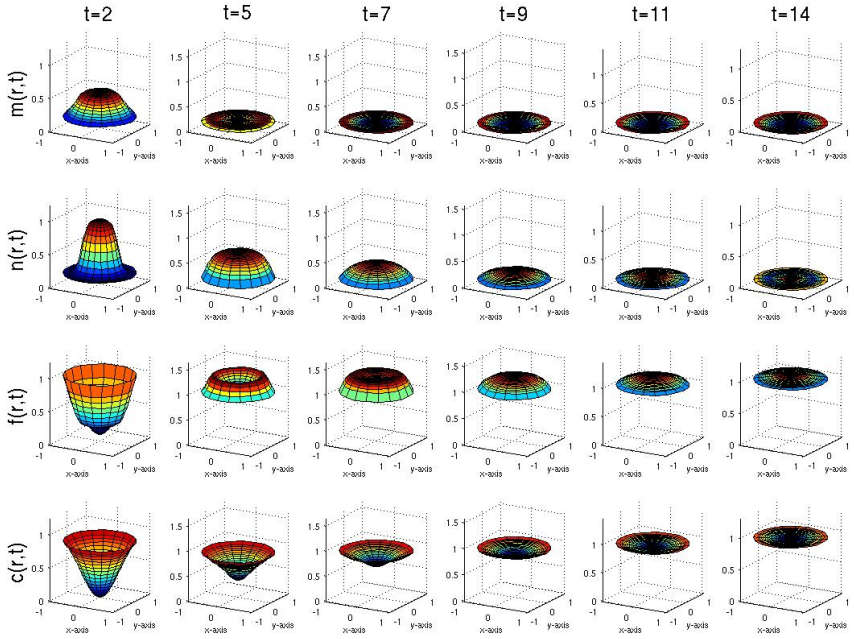

(b) 3-Dimensional rotational plots about axis of symmetry

Figure 5.5: Simulation of first 14 days post-injury

During the initial transient phase, inflammatory cells appear to be the sole responders to the injury. This behavior is expected, and it represents the inflammatory response associated with wound repair. During this period, inflammatory cells first diffusive into the wound at approximately 7.2 hours or 0.3 days. After this point, these cells begin to migrate into the wound via a mechanism other than diffusion. This is the Keller-Segel chemotaxis model in action. As a result, inflammatory cells begin to accumulate at the wound's center within 14.4 hours or 0.6 Days. The aggregation of inflammatory cells continues and becomes more pronounced by the end of the first day. As inflammatory cells migrate into the wound, they remove damaged tissue. During the initial phase, the removal is very subtle, but by the end of the first day, it becomes clearly apparent, particularly at the wound center where the normalized density of tissue damage becomes less than unity.

The intermediate phase associated with our solution is illustrated in Figure 5.5. Here, we provide the simulations results for a two week period following the initial 24 hours post injury. In this figure, we examine the response of our four unknowns for days $2, 5, 7, 9, 11$ and 14. The inflammatory response continues to gain strengthen during the initial time points of this phase. Inflammatory normalized cell density reaches it maximum value during the simulation at day 2. As a result, the tissue damage profile reduces to approximately 50% of its initial value at the wound center. In addition, we begin to see the first indications of fibroblast infiltration. In our model, fibroblasts respond to inflammatory cell gradients via the Keller-Segel model. Because inflammatory cells release factors associated with fibroblast chemotaxis, we assume that cytokine gradients may be approximated using normalized inflammatory cell density. Consequently, fibroblasts appear to aggregate near the inflammatory cell curve's inflection point. This is where the inflammatory cell gradient reaches its maximum value and is approximately the midway point between the wound's center and edge.

At Day 5, the inflammatory response begins to subside but spreads outward shifting

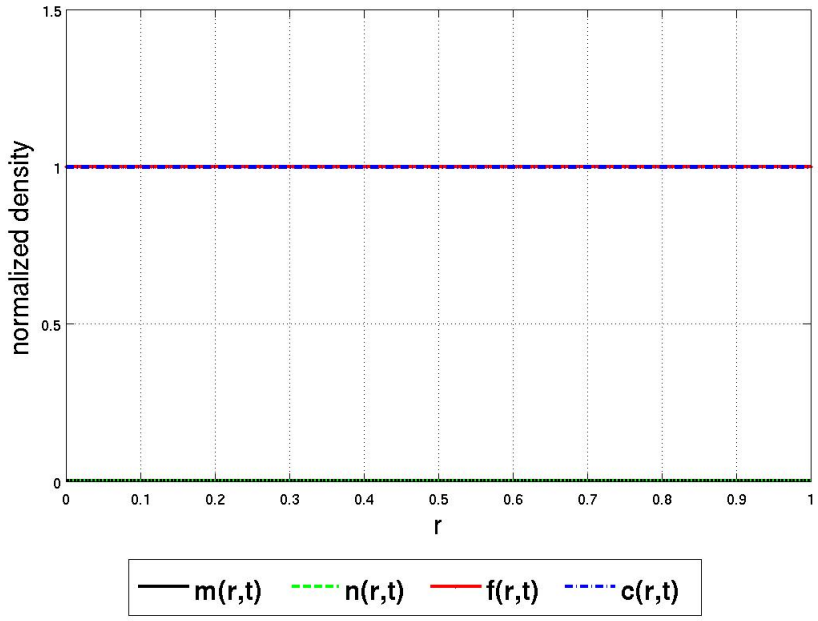

Figure 5.6: Simulation values at $t = 1000$ days

its gradient in the direct the wound boundary. Fibroblasts respond to this spatial shift. As fibroblasts continue to migrate into the wound, they follow the inflammatory cell gradient. As a result, their levels peak in the vicinity of this region, and they slowly diffuse from this point toward the center of the wound. This process continues into days 7 and 9 where fibroblast levels peak. During this time-frame, fibroblasts deposit new collagen matrix. As this new collagen approaches the nominal level in healthy tissue, fibroblast activity subsides. This process continues as both of these unknowns converge toward unity, which is depicted in the final plot shown in Figure 5.5.

After the initial two week period, there is little activity with regard to repair in the wound. Figure 5.6 illustrates this point. This figure displays activity during the steady state phase. Here, we plot the curves associated with all unknowns at $t = 1000$ days after the initial injury. As time increases, the four unknowns slowly converge on the homogeneous steady

state solution. This solution represents the repaired state, where $(\bar{m}, \bar{n}, \bar{f}, \bar{c}) = (0, 0, 1, 1)$.

5.5 Model Validation

Although the numeric solution presented in Figures 5.4 - 5.6 is in reasonable agreement with the characteristic values reported in Table 5.1, it is important to note that the set of parameters, which produced this solution, were selected based upon their evaluation criteria. In order words, we selected the solution based upon its performance. This simply verified that our model successfully describes the ideal behavior associated with the repair of an acute dermal wound. Now we answer the question: how well does this particular solution describe a clinical investigation carried out with the implantable system?

Oswal et. al. [41] recently reported on a wound repair study which implemented an expanded polytetraflouroethylene, ePTFE, sponge. The purpose of their investigation served to validate the results of an entropy-based automated cell nuclei segmentation and quantification algorithm. This routine automates the process of manually counting cell nuclei that have been histochemically treated for biological markers. In their examination, they compared results obtained from their algorithm with manual counts preformed by a pathologist. Their data set consisted of 21 immunohistochemically stained images belonging to a single patient. Images were treated with Hematoxylin & Eosin (H&E), cluster of differentiation 68 (CD-68) or alpha-smooth muscle actin (α-SMActin) stains. Samples were acquired from human tissue sections derived from the ePTFE implant. Tubes were implanted subcutaneously into the upper arms of a healthy volunteer subject, and were removed at 5, 7 and 14 days after surgical implantation.

In this study, macrophages were identified by the presence of a specific cytoplasmic granule referred to as CD-68, and fibroblasts were characterized by Hematoxylin & Eosin (H&E) stain. In addition to this data, we have acquired results from this study (not published)

Cell Type	Time	Manual Quantification	Normalized Manual	Simulation	Normalized Simulation	Relative Error
fibroblasts	5	86	0.61	1.12	0.89	0.28
	7	141	1.00	1.26	1.00	0
	14	105	0.74	1.04	0.83	0.08
macrophages	5	99	0.69	0.55	0.89	0.34
	14	143	1.00	0.09	0.15	0.85
collagen	5	90	0.54	0.62	0.65	0.11
	7	145	0.87	0.77	0.80	0.07
	14	167	1.00	0.95	0.99	0.01

Table 5.4: Comparison simulation versus empirical data

which quantify the degree of collagen deposition in ePTFE cross sections courtesy of Dr. Robert F. Deigelmann. These images where treated with a trichrome stain, which is a specific marker for collagen. Table 5.4 summarizes the results obtained from these two sources.

According to Oswal, macrophages and fibroblasts were expressed in terms of the total number of cell nuclei per cross section of ePTFE sponge. Alternatively, collagen deposition in these cross sections was quantified by the total color intensity of pixels. These measurements reflect total values with no spatial dependence. For this reason, we computed the total value associated with a given unknown over the entire domain at each time point using composite trapezoidal integration. The composite trapezoidal rule is

$$\int_0^1 u(x,t)dx = \frac{\Delta x}{2}\left[u(0,t) + 2\sum_{i=1}^{n-1} + u(1,t)\right], \tag{5.10}$$

where n and δx were set to 200 and 0.05, respectively. We then normalized a given data set from either the clinical investigation or our simulation with its respective maximum value to account for discrepancy between units. Table 5.4 compares the final results of process. Here, the normalized values, which correspond to a particular unknown, are reported for each data set for days 5, 7 and 14. In addition, we computed the relative

error between the respective data sets. We report these values in the last two columns of Table 5.4. Examination of these calculations indicate that our model accurately predicts the maximal response associated with fibroblasts and collagen deposition; however, there is only a qualitative level of agreement with the off peak responses associated with fibroblasts. The model breaks down in its description of the inflammatory response. Comparison between the macrophage levels for both days 5 and 14 show the largest points of disparity among our model and the empirical data set. For this case, it appears that macrophage infiltration lasts substantially longer than the 7 day period we reported in Table 5.1. Since we used this point as a characteristic value for our evaluation criteria, it is understandable why our results do not agree with these empirical points. Finally, our model's best performance occurs in its depiction of new collagen deposition. Here the greatest disparity occurs at day 5 where we report an absolute error of 20%.

As a final comparison, we plot each empirical data point against its respective value obtained from the numerical solution. Figure 5.7 displays the normalized values associated with each data set over a 16 day period. Here, we report total normalized levels of each unknown that was recorded in Table 5.4. Figure 5.7 reports these values for macrophages, fibroblasts and collagen deposition, respectively.

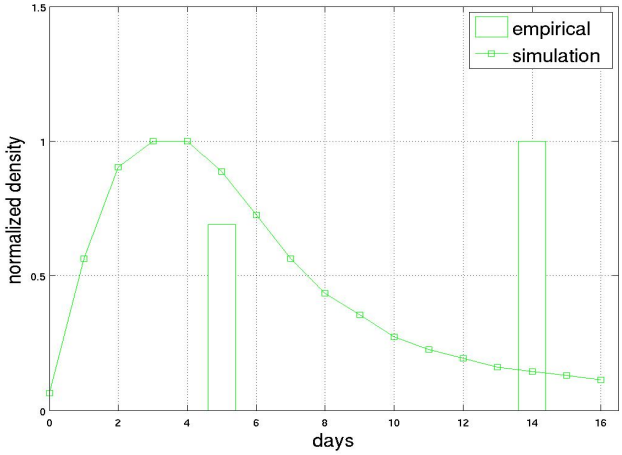

(a) inflammatory cell comparison

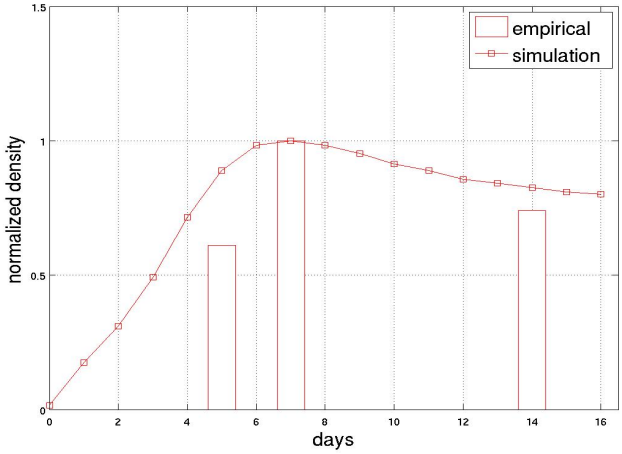

(b) fibroblast cell comparison

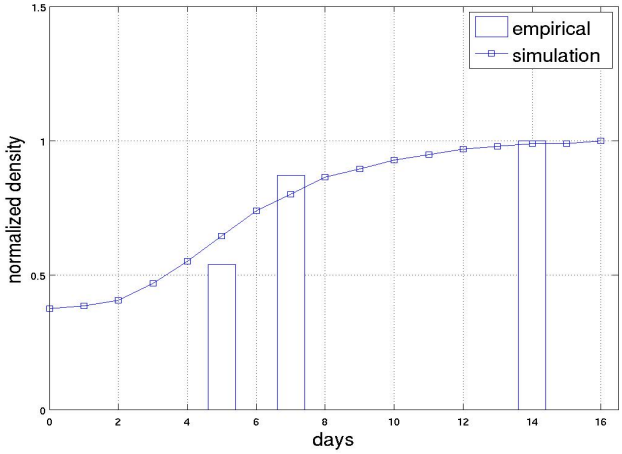

(c) collagen deposition comparison

Figure 5.7: Comparison of simulated versus empirical data

Discussion

We have created a basic PDE model which describes the repair of an acute dermal wound within the confines of human implantable systems. In our approach, we primarily focused on the fundamental mechanisms associated with the inflammatory and proliferation phases. Our system of equations accounts for the time rate of change in the density of the initial damage, inflammatory cells, fibroblasts and new collagen. The underlying mechanisms associated with unknowns in our system of equations included the rate of mitotic cell division, cell death, collagen deposition, phagocytosis and chemotaxis. We implemented fundamental mathematical techniques to account for a majority of these processes such as the first order decay, the Law of Mass Action and the logistic model. In our model, the Keller-Segel chemotactic model accounts for the reaction-diffusion processes associated with inflammatory and fibroblast cell populations during repair. The coefficients associated with our PDE model were obtained through simulations with our system equations. We carried out simulations until there was general agreement between a given solution and a set of characteristic values that we obtained from the literature. This strategy appears to have produced promising results for an initial attempt toward modeling implantable systems.

Although our wound repair system predicts the general progression for most of the unknowns it models, there were cases where the model deviated from data sets obtained from both theoretical and empirical perspectives. The inflammatory response appears to be the major exception in this last regard for both cases.

From a theoretical venue, the inflammatory response does not match all characteristic

values obtained from our literature review. In our system, this response initiates within a reasonable period; however, inflammatory cell activity last appreciably longer than reported. For a typical acute dermal wound, the inflammatory phase usually subsides approximately seven days after the initial infraction [2], [2] [5]. In our system, it is difficult to determine exact intervals of this type for all unknowns. This is because of the continuous behavior associated with all variables in our model; however, according to our verification criteria, inflammatory cells maintain 10% of their peak value 13.4 days after the start the simulation. This compares poorly with data reported within the literature for an acute inflammatory response. The situation might be correct by the inclusion of a decay term that represents inflammatory cell death. We did not include this term in the inflammatory cell equation because we hypothesized that the death of inflammatory cells from phagocytosis should dominate their background decay rate.

When we compared the results produced by our system with empirical data obtained from ePTFE implants [41], similar trends emerged between experiment and numerical solution. Our model accounts for the general behavior of fibroblasts, myofibroblasts and collagen deposition for 5, 7 and 14 days after implantation. In this regard, there is particularly good agreement between the peak responses for these data sets. The closest agreement between any data set occurs with the deposition of new collagen. We computed the relative errors for collagen deposition for days 5, 7 and 14 as 0.11, 0.07 and 0.01, respectively. Although we had a reasonable prognosis for these unknowns, our model's prediction for macrophages (i.e. inflammatory cells) proved problematic. Data obtained from Oswal et al. showed that macrophages remained at appreciable levels 14 days after implantation. Although there are only two points in their data set for macrophages, this point represents the peak value. In our model, inflammatory cells attain their accumulated peak value on day three. We selected parameters for our system of equations that would yield outcome consistent with data collected from our literature review [1] - [3], [5], [6], [9], [11], [12],

[37]. Hence this empirical observation is also in disagreement with those sources.

Human implantable models present tremendous opportunities for applied mathematicians interested in applying their skills in the field of biomathematics. Implants greatly simplify the mathematics required to describe the repair process because they minimize the modeling of complex features associated with wound healing. Furthermore, these empirical systems provide valuable data, which is collected in an controlled environment. Consequently, the results of these studies can be used to validate any hypothetical mathematical system which attempts to model certain aspects of the repair process, such as the inflammatory response or fibroplasia. These mathematical systems can in turn play a valuable role in the study of wound healing. For instance, mathematical models offer a noninvasive approach to studying the dynamics of healing in human studies. These system allow for the study of hypotheses and therapies to be examined before clinical implementation [19]. A numerical model can increase the success of clinical trails and aid in the understanding of disorders associated with abnormal healing such as hypertrophic scar formation and chronic ulcers.

In this work, we have taken an important first step toward developing a basic mathematical system that describes the repair of acute dermal wounds within the context of implantable systems. In future work, we hope to incorporate additional features into our PDE model. These features would include accounting for the effect of low tissue oxygenation along with the inclusion of a pathogen term. In addition, we should also account for the side affects of inflammation such as tissue damage. Furthermore, it would be advisable to include a cytokine equation rather than assume that gradients associated PDGF and TGF-α maintain levels of proportionality with the cell types that produce these cytokines. Finally, since the inflammatory response in our model has proved questionable, it might be advantageous to divide this response into two terms. The remedy would consist of separate equations for neutrophils and macrophages.

Bibliography

Bibliography

[1] R. F. Diegelmann and M. C. Evans, *Wound healing: an overview of acute, fibrotic and delayed healing*, Frontiers in Bioscience 2004; 9: 283-289.

[2] J. L. Monaco and W. T. Lawrence, *Acute wound healing an overview*, Clin. Plastic Surg. 2003; 30: 1-12.

[3] G. Broughton II, J. E. Janis and C. E. Attinger, *Wound healing: an overview*, Plast. Reconstr. Surg. 2006; 117: 1es-32es.

[4] C. J. Pallister and M. S. Watson, *Hematology*, 2010: Scion Publishing. 334-336.

[5] M. Li, J. A. Norton, R. R. Bollinger, A. E. Chang, S. F. Lowry, S. J. Mulvihill, H. I. Pass and R. W. Thompson, *Essential practice of surgery, basic science and clinical evidence* 2003: Springer, 77-88.

[6] B. A. Mast and G. S. Schultz, *Interactions of cytokines, growth factors, and proteases in acute and chronic wounds*, Wound Rep. Regen. 1996; 4: 411-20.

[7] D. W. Thomas, I. D. O'Neill, K. G. Harding and J. P. Sheperd, *Cutaneous wound healing: a current perspective*, J. Oral Maxillofac Surg. 1995; 53: 442-447.

[8] S. A. Eming, T. Krieg and J. M. Davidson, *Inflammation in wound repair: molecular and cellular mechanisms*, J. of Investigative Dermatology 2007; 127: 514-525.

[9] M. Mercandetti and A. J. Cohen, Wound Healing and Repair, Medscape, April 3, 2013, Accessed May 3, 2013 http://emedicine.medscape.com/article/1298129-overview

[10] E. I. Egozi, A. M. Ferreira, A. L. Burns and R. L. Gamelli, *Mast cells modulate the inflammatory but not the proliferation response in healing wounds*, Wound Rep. Regen. 2003; 11: 46-54.

[11] D. G. Greenhalgh, *The role of apoptosis in wound healing*, International Journal of Biochemistry and Cell Biology 1998; 30: 1019-1030.

[12] W. K. Stadelmann, A. G. Digenis, G. R. Tobin, *Physiology and healing dynamics of chronic cutaneous wounds* Am. J. Surg. 1998; 176(Suppl 2A): 26S-38S.

[13] R. A. F. Clark and P. M. Henson, *The molecular and cellular biology of wound repair*, 1988: Plenium Press, New York, 3-34.

[14] J. Breiter-Hahn, A. G. Matoltsy and K. S. Richards, *Biology of the integument: vertebrates, vol. 2*, 1986: Springer-Verlag, Berlin, 443-471.

[15] J. Breiter-Hahn, A. G. Matoltsy and K. S. Richards, *Biology of the integument: vertebrates, vol. 2*, 1986: Springer-Verlag, Berlin, 443-471.

[16] J. Seoka,, H. S. Warren, A. G. Cuenca,, M. N. Mindrinos, H. V. Baker, W. Xu, D. R. Richards, G. P. McDonald-Smith, H.Gao, L. Hennessy, C. C. Finnerty, C. M. LÃşpez, S. Honari, E. E. Moore, J. P. Minei, J. Cuschieri, P. E. Bankey, J. L. Johnson, J. Sperry, A. B. Nathens, T. R. Billiar, M. A. West, M. G. Jeschke, M. B. Klein, R. L. Gamelli, N. S. Gibran, B. H. Brownstein, C. Miller-Graziano, S. E. Calvano, P. H. Mason, J. P. Cobb, L. G. Rahme, S. F. Lowry, R. V. Maier, L. L. Moldawer, D. N. Herndon, Ronald W. Davis, W. Xiaoa and R. G. Tompkins , *Genomic responses in mouse models poorly mimic human inflammatory diseases*, PNAS, 2013; 110: 3507-3512.

[17] J. A. Thackham, D. L. S. McElwain and I. W. Turner, *Computational approaches to solving equations arising from wound healing*, J. Theor. Biol. 2006: 242; 220-236.

[18] A. Reynolds, J. Rubin, G. Clermont, J. Day, Y. Vodovotz and G. B. Ermentrout, *A reduced mathematical model of the acute inflammatory response: I. Derivation of model and analysis of anti-inflammation*, J. Theor. Biol. 2006; 242: 220-236.

[19] M. B. Menke, J. W. Cain, A. Reynolds, D. M. Chan, R. A. Segal, T. M. Witten, D. G. Bonchev, R. F. Diegelmann and K. R. Ward, *An in silico approach to the analysis of acute wound healing*, Wound Rep. Reg. 2010; 18: 105-113.

[20] J. A. Sherratt and J. D. Murray, *Models of epidermal wound healing*, Proc. R. Soc. Lond. B 1990; 241: 29-36.

[21] J.A. Sherratt and J.D. Murray, *Mathematical analysis of a basic model for epidermal wound healing*, J. Math. Biol. 1991; 29: 389-404.

[22] F. J. Vermolen and E. van Baaren and J. A. Adams, *A simplified model for the growth factor induced healing of wounds*, Mathl. Comput. Modelling 2006; 44: 887-898.

[23] J. A. Adam, *A simplified model of wound healing (with particular reference to the critical size defect)*, Mathl. Comput. Modelling 1999; 30: 23-32.

[24] J. S. Arnold and J. A. Adams, *A simplified model of wound healing II (the critical size defect in two dimensions)*, Mathl. Comput. Modelling 1999; 30: 47-60.

[25] J. S. Arnold and J. A. Adams, *A simplified model of wound healing III (the critical size defect in three dimensions)*, Mathl. Comput. Modelling 2001; 34: 385-392.

[26] C. Xue, A. Friedman and C. K. Sen, *A mathematical model of ischemic cutaneous wounds*, PNAS 2009; 106: 16782-16787.

[27] A. Friedman and C. Xue, *A mathematical model of chronic wounds*, Mathematical Biosciences and Engineering 2011; 8: 253-261.

[28] S. M. Alaish, D. A. Bettinger, O. O. Olutoye, L. J. Gould, D. R. Yager, A. Davis, M. C. Crossland R. F. Diegelmann and I. K. Cohen, *Comparison of the polyvinyl alcohol sponge and expanded polytetrafluoroethylene subcutaneous implants as models to evaluate wound healing potential in human beings*, Wound Rep. and Reg. 2003; 11: 46-54.

[29] L. N. Jorgensen, *Collagen deposition in the subcutaneous tissue during wound healing in humans: a model evaluation*, APMIS Suppl. 2003; 115: 9-56.

[30] I. R. Lapidus and R. Schiller, *A mathematical model for bacterial chemotaxis*, Biophysical Journal, 1974; 14: 825-834.

[31] I. R. Lapidus and R. Schiller, *Model for the chemotactic response of a bacterial population*, Biophysical Journal, 1976; 16: 779-789.

[32] E. F. Keller, L. A. Segel, *Initiation of slime mold aggregation viewed as an instability*, J. Theor. Biol. 1970; 26: 225-234.

[33] E. F. Keller, L. A. Segel, *A model for chemotaxis*, J. Theor. Biol. **30** 225-234, 1971.

[34] E. F. Keller, L. A. Segel, *Traveling bands of chemotactic bacteria: a theoretical analysis*, J. Theor. Biol. 1971; 30: 377-38

[35] T. Hillen and K. J. Painter, *A user's guide to PDE models for chemotaxis*, J. Math. Biol. 2007; 58: 183-217.

[36] Leah Edelstein-Keshet, *Mathematical models in biology* 2005: SIAM, 496-507.

[37] J. Gailit and R. A. F. Clark, *Wound repair in the context of extracellular matrix* Current Opinion in Cell Biology 1994; 6: 717-725.

[38] R. F. Sincovec and N. K. Madsen, *Software for nonlinear partial differential equations*, ACM Trans. on Math. Software 1975; 1: 232-260.

[39] R. F. Sincovec and N. K. Madsen, *PDEONE, solutions of systems of partial differential equations, Algorithm 494*, ACM Trans. on Math. Software 1975; 1: 261-263.

[40] J. L. Weatherwax, *Solving PDE's with Octave: PDEONE & the Runge Kutta Chebyshev ODE integrator, rkc.f* 2005, Accessed July 15, 2013 http://waxworksmath.com/Software/pdeone_rkc.html.

[41] V. Oswal, A. Belle, R. Diegemann, and K. Najarian *An entropy-based automated cell nuclei segmentation and quantification: application in analysis of wound healing process*, Computational and Mathematical Methods in Medicine 2013; ??

Appendix A

Summary of Model Paramters

Parameter	**Hypothetical Units**	**Notional Units**	**Definition**
m	$volume$	μm^{-3}	*Density of damaged tissue*
M_0	$volume$	μm^{-3}	*Density of initial tissue damage*
μ_{mn}	$volume \cdot time^{-1}$	$\mu m^3 \cdot d^{-1}$	*Consumption rate of damaged tissue by inflammatory cells*
n	$volume$	μm^{-3}	*Density of activated inflammatory cells*
N_a	$volume$	μm^{-3}	*Background density of activated inflammatory cells*
D_n	$space^2 \cdot time^{-1}$	$\mu m^2 \cdot d^{-1}$	*Activated inflammatory cell diffusion constant*
χ_n	$space^5 \cdot time^{-1}$	$\mu m^4 \cdot d^{-1}$	*Activated inflammatory cell chemotactic constant*
μ_{nm}	$volume \cdot time^{-1}$	$\mu m^3 \cdot d^{-1}$	*Death rate of inflammatory cells from consumption of damage tissue*
f	$volume$	μm^{-3}	*Concentration of fibroblasts*

F_0	$volume$	μm^{-3}	*Nominal concentration of fibroblasts in healthy tissue*
D_f	$space^2 \cdot time^{-1}$	$\mu m^{-2} \cdot d^{-1}$	*Fibroblast diffusion constant*
χ_f	$space^5 \cdot time^{-1}$	$\mu m^5 \cdot d^{-1}$	*Fibroblast chemotactic constant*
k_f	$time^{-1}$	d^{-1}	*Fibroblast growth rate constant*
μ_f	$time^{-1}$	d^{-1}	*Fibroblast death rate constant*
k_c	$volume \cdot time^{-1}$	$\mu m^3 \cdot d^{-1}$	*Rate of collagen deposition*
μ_{cn}	$volume \cdot time^{-1}$	$\mu m^3 \cdot d^{-1}$	*Fibroblast death rate constant*

Appendix B

Code List

```
function [pl,ql,pr,qr] = bc(xl,ul,xr,ur,t)

 % bc: matlab function M-file that defines boundary conditions
 % for a system of two PDE in time and on space dimension.

 global Cr; global Wo; global Rf;

 pl = [0; 0; 0; 0];
 ql = [1; 1; 1; 1];
 pr = [0; ur(2) - Cr*ur(1); ur(3) - Wo; 0];
 qr = [1; 0; 0; 1];

end

function value = icfun(x)

 % initial conditions: matlab function M-file that defines initial conditions
 % for a sytstem of two PDE in time and one space variable.

 global Vo;  global Cv; global Co;
 global Cu;
 global Wo; global Cw;
 global Rf;
```

```
 value = [ Vo*exp(Cv.*(x).^2) + Co; ...
           (Vo*exp(Cv) + Co).*exp(Cu.*(1-x)); ...
           Wo.*exp(Cw.*(1-x)); ...
           Rf - (Vo*exp(Cv.*(x).^2) + Co) ];

end

function [c,b,s] = pdefun(x,t,u,ux)

 % globalvariable definitions see pdepe_script.m
 global Uo; global Wo;
 global Dv; global Mv;
 global Du; global Xu; global Uf; global Mu;
 global Dw; global Xw; global Wf; global Kw; global Mw;
 global Dr; global Rf; global Kr; global Mr;

 % wound healing system with keller-segal chemotaxis
 c = [1; 1; 1; 1];

 b = [ Dv*ux(1); ...
       Du*ux(2) - u(2).*Xu.*ux(1); ...
       Dw*ux(3) - u(3).*Xw.*ux(2); ...
       Dr*ux(4) ];

 s = [ -Mv*u(2).*u(1); ...
       -Mu*u(2).*u(1); ...
       Kw.*u(3).*(2 - u(3)./Wo) - Mw*u(3); ...
       Kr.*u(3).*(Rf - u(4)) - Mr.*u(2).*u(4) ];

end

% PDEPE: MATLAB script solves the PDE
```

```
% stored in icfun.m, bc.m and pdefun.m

global Vo; global Cv; global Co; global Wo;
global Cu; global Cw;  global Cr;
global Dv; global Mv;
global Du; global Xu; global Uf; global Mu;
global Dw; global Xw; global Kw; global Mw;
global Dr; global Rf; global Kr; global Mr;

m = 1;  Xm = 1; Tm = 100; Nx = 201; Nt = 1001;
pts = Tm*[0 0.005 0.01 0.02 0.05 0.07 0.10 0.14 1.0];

Vo = 1.0; Uo = 1; Wo = 1;
Cv = -2; Cu = -5; Cw = -50; Co = 0; Cr = 1;

% damage equation constants
Dv = 0; Mv = 0.5;

% inflammatory equation constants
Du = 0.05; Xu = 0.7; Mu = 0.01;

% fibroblast equation constant values
Dw = 0.03; Xw = 0.1; Kw = 0.3; Mw = 0.3;

% collagen equation constant values
Dr = 0; Rf = 1; Kr = 0.3; Mr = 0.1;

x = linspace(0, Xm, Nx);
t = linspace(0, Tm, Nt);

sol = pdepe(m,@pdefun,@icfun,@bc,x,t);
```